University of Chemical Technolog and Metallurgy

Faculty of Metallurgy and Materials Science

Department of Silicate Technology

eng. Dimitar Krasimirov Dimitrov

Topic

"FUNCTIONAL THIN FILM COATINGS CONTAINING GRAPHENES"

Thesis Abstract

of dissertation

for educational and scientific title "doctor"

Scientific field 5.10. Chemical technologies (Technology of silicates, binders and refractory non-metallic materials)

Thesis advisor: Prof. dr. eng. Anna Staneva

Scientific committee:

1. - chairman
2. ……. - reviewer
3. ……. - reviewer
4. …….
5. …….

Sofia, 2025

The dissertation consists of …… pages, contains ….. figures and …….. tables. …….. sources have been cited.

The work presented has been discussed and accepted for public defence at the ……. assembly of the scientific staff of the department for Silicate technology on …….

The public defence of the dissertation will take place on …… at ……, room ……, building ….. of the UCTM.

All materials can be accessed through the UCTM website, as well as from the department for Scientific activity (room 406, building A of the UCTM), by anyone concerned.

INTRODUCTION

Graphene and graphene materials are nanostructures that combine promising electrical, thermal, optical, mechanical and electronic properties, which make them an attractive material for both technical and medical applications. The development of suitable compositions of thin-film coatings with their participation allows for the production of new materials with potential for application in electronics, medicine, optics, energy storage, and more. High electrical conductivity, mechanical strength, thermal conductivity, good optical and other properties, are a prerequisite for promising applications in portable electronics and hybrid electric vehicles, for the creation of a new generation of batteries, supercapacitors, etc. Their biocompatibility, large specific surface area, antimicrobial and electronic activity cause increased interest in medical applications, such as diagnostics and treatment of cancer, drug delivery, antibacterial and antiviral agents, biosensors, biomaterials for wound healing, as well as for tissue engineering, etc.

Thin-film coatings have a rich history and are an indispensable component of many modern materials. They are responsible for the functioning of practically every modern optical element. The methods of their preparation are inextricably linked to those used in electronics, photonics, laser technology, corrosion protection.

Thin-film coatings with added graphene materials are a promising field of work, since many of the properties of such composite materials are unexplored, and the benefits and challenges have yet to be investigated.

The resistance of microorganisms to conventional antimicrobial agents (antibiotics) is a serious challenge in healthcare. Graphene oxide (GO) has been proven as an effective antimicrobial agent against antibiotic-resistant microorganisms. There is evidence of cross-resistance to antimicrobial nanoparticles, but not between nanostructured materials and conventional antibiotics. Of particular interest is the antimicrobial activity of graphene against resistant strains and the disruption of the biofilm formation process.

This motivated the team's interest in this type of materials and predetermined the goal of the doctoral dissertation.

AIM OF THE DOCTORAL DISSERTATION

To produce and characterize functional thin-film coatings involving graphene materials with potential for application in optics, as protective, and antibacterial coatings.

TASKS:

1. To obtain and characterize thin-film optical coatings according to predefined parameters.
2. To study and test various materials for inclusion in thin film coatings.
3. To obtain and characterize polymer composites with the participation of graphene materials.
4. To test the application of a polymer coating of Poly(Bisphenol A- co -epichlorohydrin) on samples by dip coating method.
5. To study and optimize a route for processing the substrates.
6. To obtain RGO by an appropriate method.
7. To obtain nanoparticles to be included in composites – ZnO, $ZnTiO_3$.
8. To test various methods of dispersion of graphene materials in polymer composites.
9. To select and apply appropriate methods for characterizing the resulting coatings.

I. EXPERIMENTAL

MATERIALS AND EQUIPMENT USED

Table 1. Materials and equipment.		
For substrate treatment		
Chemicals	Origin	Equipment
Methanol	Valerus	Ultrasinug cleaning and dip coating installation SCL-HPP5
Ethanol	Valerus	
Isopropanol	Valerus	
NaOH	Valerus	
Surfactant LC-40	SCL Int.	
DI water	Ivylens	
Pressurized dry air	Ivylens	
For epoxy and thin film coatings		
Bisphenol-a-epicholohyrin (152-72-NT)	SCL Int.	IR-chamber, dryer.
MgF_2	Coerent Italy	Vacuum chamber MCX – 380
Ti_3O_5	SatisLoh	Molybdenum liner
SiO_2	SatisLoh	Spectrophotometer SatisMS – 200
ZrO_2 – grey	SatisLoh	
Quartz crystal 6MHz	SatisLoh	
Ar	Ivylens	MCalc software
O_2	Ivylens	
For ZnO nanoparticle synthesis		
Zinc Acetate	Dept. Silicate Technology, UCTM	Digital scale (KERN PCB350-3)
Acetic acid		Assorted beakers
Isopropanol		Measuring glassware
For $ZnTiO_3$ nanoparticle synthesis		
Titanium ethoxide	Dept. Silicate Technology, UCTM	Ice bath
Ethylene glycol		Centrifuge
Citric acid		Glass slides
Ethanol		Glass slide covers
Zinc acetate		
For GO and RGO synthesis		
Graphite powder	Dept. Silicate Technology, UCTM	Magnetic stirrer MSH-300N
H_2SO_4		Measuring pipettes (Assistent)
$NaNO_3$		Ultrasonic reactor GEX 750 W
$KMnO_4$		Crosshatch blades
H_2PO_4		Origin software
H_2O_2 (30 %)		Agate ball mill Fritsch, Analisette 3 SPARTAN, Pulverisette
HCl (1M)		
NaOH		
$NaBH_4$		Buchner funnel
Distilled water		

7. EXPERIMENTAL RESULTS AND DISCUSSION

7.1. SYNTHESIS OF THIN FILM OPTICAL COATINGS ON POLYMER SUBSTRATES

The presented experiment follows the following sequence:

• Selection of materials for the composition of a thin-layer coating;

• Development of a recipe (design) with a certain ratio of the thicknesses of the layers included in the coating using computational software and obtaining an optical plot according to a preliminary assignment;

• Preparation of substrates and synthesis of the coating in a vacuum chamber MCX – 380;

• Investigation of the reflective properties of the coating using a spectrophotometer.

Preparation of the substrates.

For thin film synthesis, it is essential to work in a clean room with very low levels of dust, controlled airflow, temperature and humidity. This is necessary to avoid the inclusion of moisture or traces of dust in the product.

The substrates used, made of CR-39 material, have a refractive index of 1.48. There are manufacturing defects on their surface – traces of polishing, scratches, inclusions. The material itself has poor wear resistance and unacceptably poor adhesion with materials such as the oxides that will be used. This is the reason for its slow market penetration. Nowadays, these problems have been largely solved by applying hard lacquer coatings. They are also considered to be entireflective, since the filling of microcracks and scratches on the surface leads to better transmittance. The lenses become more wear-resistant and the adhesion with inorganic coatings is improved significantly. The hard coating used is a bisphenol-a based epoxy, which will be important in following experiments.

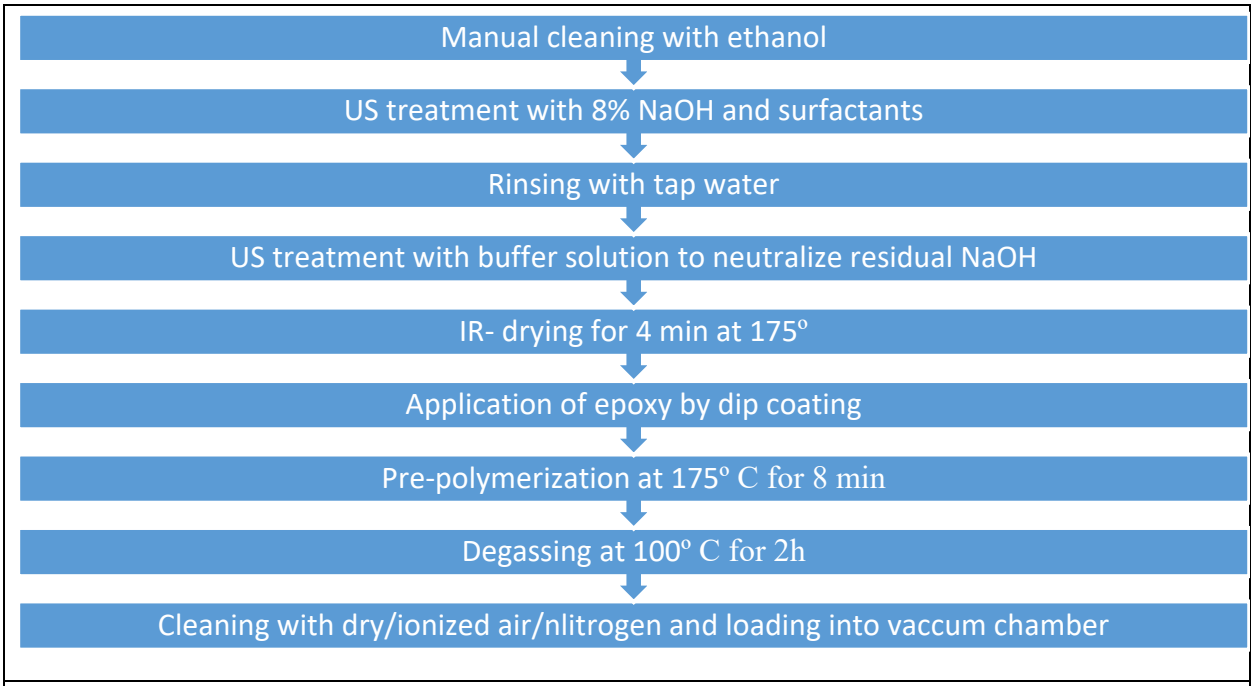

Figure 1. Substrate treatment and application of thin film coating.

In this case, the complete preparation of the substrates was carried out according to Figure 1. The substrates treated in this way have a refractive index of 1.52 and are ready for coating in a vacuum chamber.

Measurement methodology

The SNP-200 spectrophotometer used measures only the reflection values. This leads to the disadvantage when working with transparent substrates that the graph contains noise from the "back" side of the lens. In order to eliminate and obtain the absolute reflection value from the treated side, the other side must be darkened. This was achieved by sandblasting the surface and its subsequent coloring (Fig. 2)

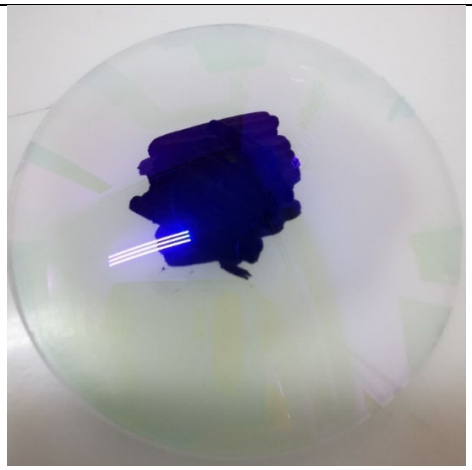

Fig. 2. Lens prepared for measurment

As with any measuring instrument, calibration is required before each measurement. This is achieved in three steps:

• "dark" measurment – the spectrophotometer is directed towards a dark non-reflective surface;

• Measurement on a reference surface – this is a surface of the same material, uncoated, darkened in the described way;

• Measurement of the sample.

7.1.1. SINGLE LAYER AR – COATING

To obtain a single-layer anti-reflective coating, we use the classic example of a thin layer of MgF_2 coating on oxide glass with n=1.5. MgF_2 has very poor adhesion to polymer substrates and is therefore not used in industry. We choose a reference wavelength of λ=550nm. This step is necessary because the refractive index of the materials depends on the wavelength. In the case of MgF_2 at 550nm, n=1.379. Entering this value into the equation for the reflection coefficient, we expect R=1.3% at 550 nm. This is also confirmed by the theoretical curve (Fig.3a). To calculate the required layer thickness, we need to divide ¼ λ by the refractive index. The full characteristics of the coating are presented in Table 2:

Table 2. Preliminary values for single layer AR coating of MgF_2 on a CR-39 substrate.		
		Refractive index at 550 nm
Substrate	CR- 39	$n_{суб}$=1.50
Medium	Air	$n_{ср}$=1
Coating	MgF_2	$n_{сл}$=1.379
ε	10%	
R	1.3%	
Physical thickness	D=99.717nm	

The coating has been successfully applied and its reflective properties are shown in Fig. 3. and comparison with the theoretical model:

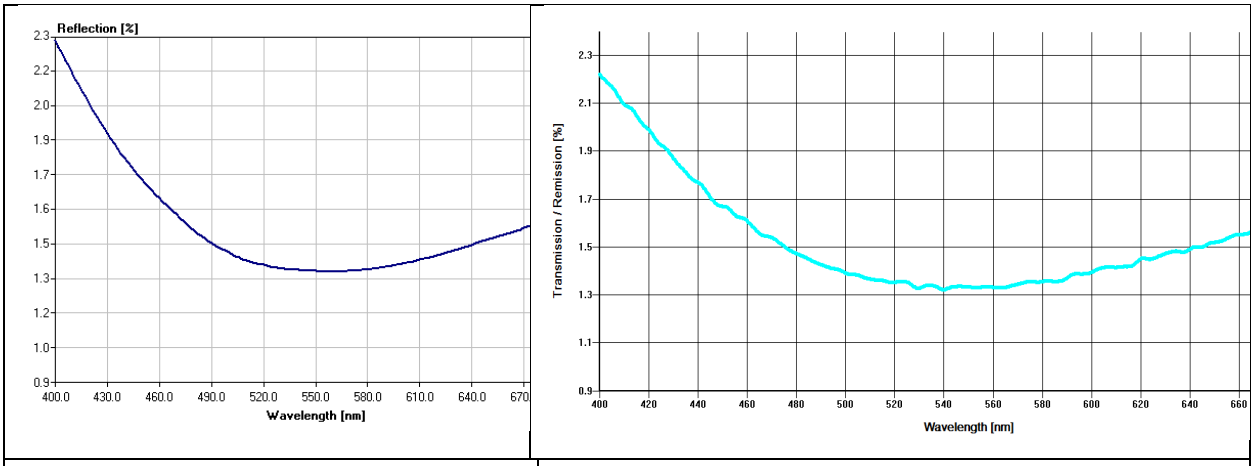

Figure. 3a. Theoretical model	b. practical measurrment

The expected minimum is observed at 550 nm with a reflectance value of just over 1.3%. Although the coating achieves lower reflectance levels compared to the uncoated substrate, two- or three-layer coatings are now easily achieved, where the improvements far outweigh the complexity of their design and synthesis.

7.1.2. THREE-LAYER AR COATING.

To overcome the shortcomings of the single-layer AR coating of MgF_2 – namely, its inapplicability on polymer lenses and the high value of residual reflection – a three-layer AR coating has been developed, again based on quarter-wave layers. The most popular materials in the industry have been used – SiO_2, Ti_3O_5 and ZrO_2. The coating itself has a characteristic W-curve with a peak of residual reflection at the reference wavelength. The position of this peak also plays the part of a kind of quality control – if it is shifted relative to the theoretical model, it means either that the thicknesses of the layers have not been achieved accurately, or that one of the layers has a changed refractive index – an indication of disturbed reaction conditions and a prerequisite for the coating to be unstable. By reverse engineering the optical curve of the resulting coating, the problematic layer can be traced.

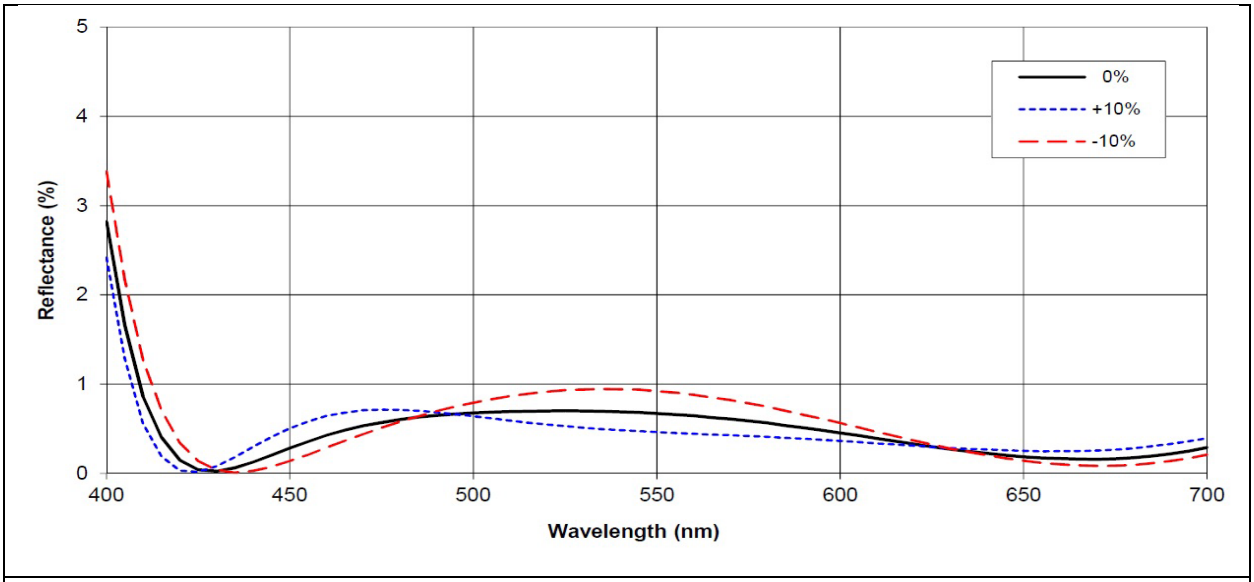

Figure. 4. Effect of thickness deviation of one layer on the optical properties of a coating.

Table 3 shows the characteristics of the developed three-layer AR coating. The starting thickness is 530nm and there is expected to be a peak of residual reflection R=1%. This means for the user the presence of glare in the lens:

Table 3. Tee-layer AR coating design

Material	Refractive index at 550 nm	Thickness
CR - 39	1.52	massive
ZrO_2	2.07	60.44nm
Ti_3O_5	2.24	55.804nm
SiO_2	1.48	84.342nm
Air	1	massive

The coating was successfully synthesized, and the results of the spectrophotometer measurements were compared with the theoretical graph in Fig. 5:

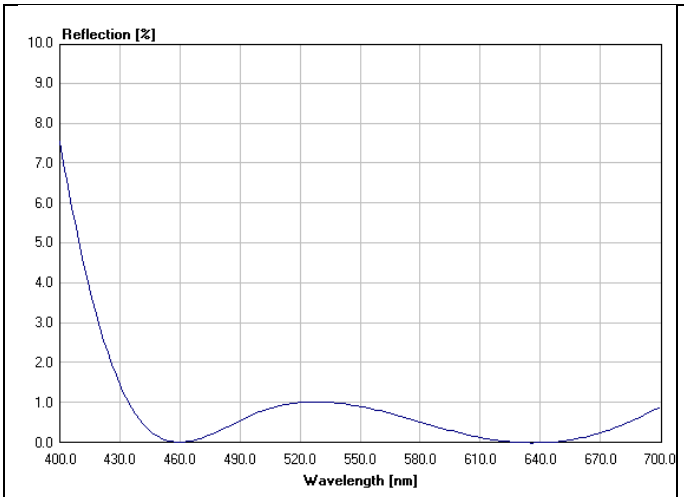

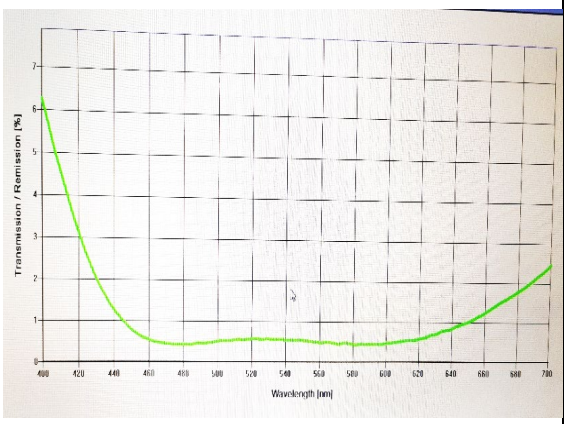

Figure 5a. Theoretical model | b. practical measurement

7.1.3. REFLECTIVE COATINGS.

Mirror coatings based on quarter-wave layers are based on the use of materials with a higher refractive index than the substrate. Another necessary condition is the correct arrangement of the layers - the layer with the highest refractive index must be at the interface with the medium. The development of a mirror coating is also a good opportunity to consider another property of quarter-wave layers, namely their multiplicity. The condition for constructive interference will also be fulfilled at a layer thickness d=k.1/4λ in cases where k is an odd number. However, the higher the value of k we use, the narrower the peak we will obtain at the reference wavelength. This is useful in the design of coatings with more stringent requirements for optical characteristics. However, the synthesis of thicker layers faces more difficulties in their uniformity and ensuring good adhesion. To study with these phenomena, two mirror coatings have been synthesized at a reference wavelength of λ=600 nm. The first with a k value of 1, and the second with k=3. Although the maximum reflection in both cases is at 600 nm, the difference in the width of the peak leads to a radically different visual result.

Table 4. Three-layer mirror coating with κ=1

Material	Refractive index at 600 nm	Thickness
CR - 39	1.52	massive
Ti_3O_5	2.22	67.72 nm
SiO_2	1.48	101.25 nm
Ti_3O_5	2.22	67.72 nm
Air	1	massive

The coating was successfully obtained and measured. A comparison with the theoretical model is shown in Fig.6.

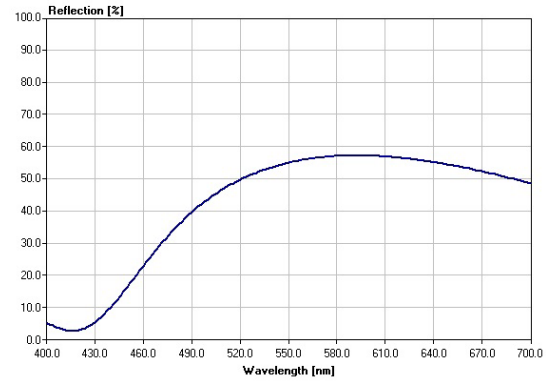

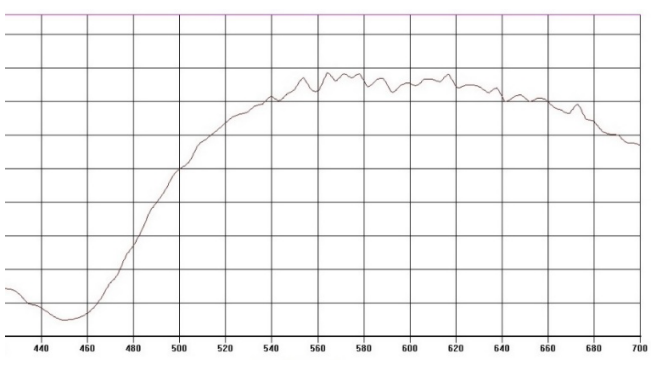

Figure 6a. Theoretical curve	b. practical measurement

For the second mirror coating, the same materials were used in the same sequence. The only difference is that the physical thickness was multiplied by a factor of 3.

Table 5. Three-layer mirror coating with κ=3		
Material	Refractive index at 600 nm	Thickness
CR - 39	1.52	Massive
Ti_3O_5	2.22	203.160 nm
SiO_2	1.48	304.65 nm
Ti_3O_5	2.22	203.160 nm
Air	1	Massive

The coating was obtained and measured. A comparison with the theoretical model is shown in Fig.34.

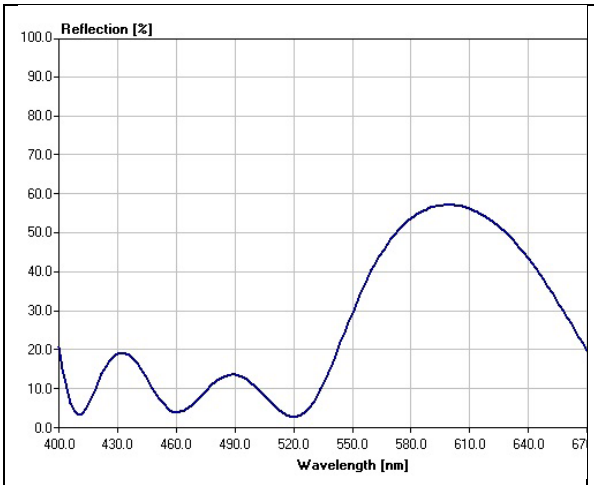

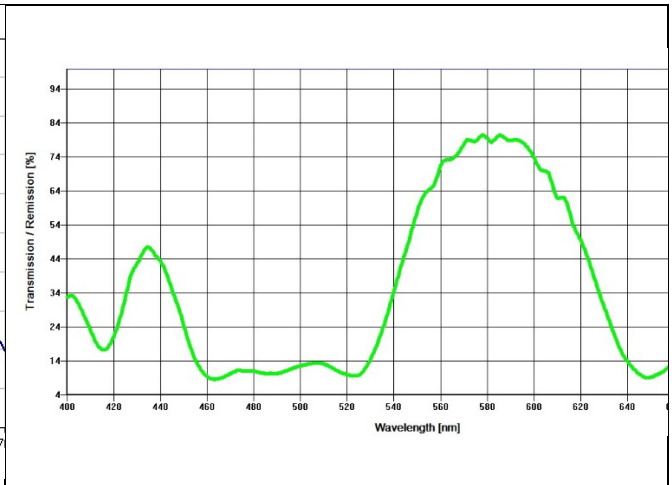

Figure 7a. Theoretical curve	b. practical measurement

A shift of the peak to the right is observed, as well as partial extinction of the secondary harmonics. This is explained by the failure to reach the required thickness of layer 2 – SiO_2. The absolute values of the measurement are inflated due to the non-treatment of the uncovered surface. A curve with a diminished thickness of layer 2 by 3.33% and simulation of reflection on the back side is simulated. (Fig. 35). The graph corresponds to the experimental curve.

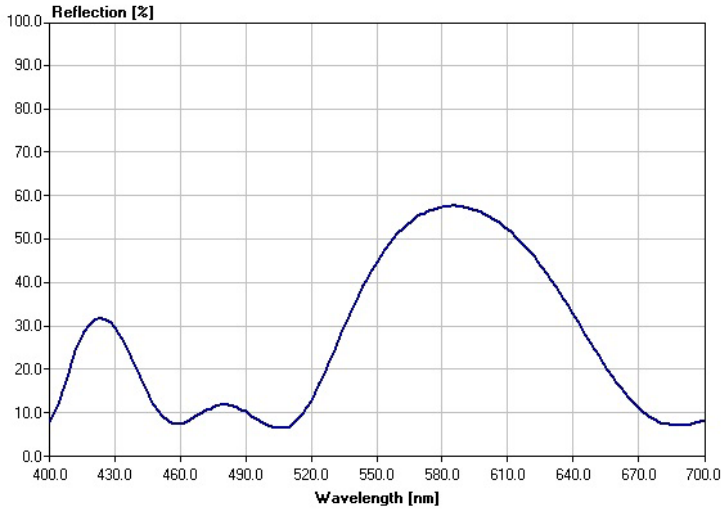

Figure 8. Theoretical model explaining the deviations.

Despite the deviation in the synthesis of the coating with k=3, a narrowing of the peak is clearly visible, compared to that of the design with k=1. Visually, the two substrates look radically different – Figure 9.

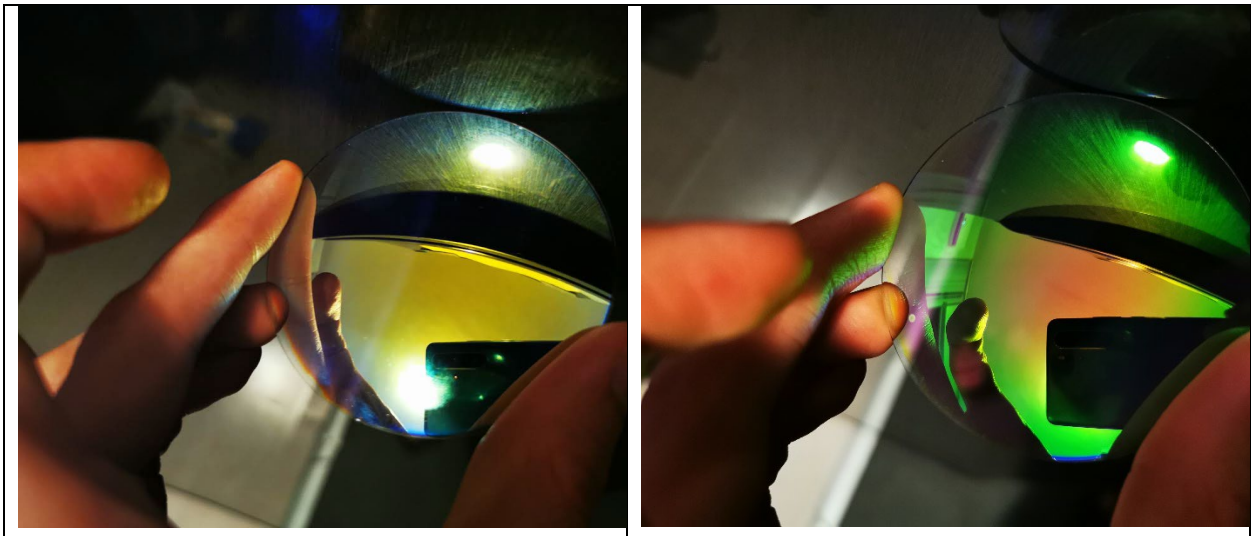

Figure 9a. Mirror coating with k=1; b. Mirror coating with k=3.

Mirror coatings are a clear example of some of the additional difficulties that thin film production technology faces:

- So far, all calculations have been based on an angle of incidence of 0º. However, the refractive index is also sensitive to this parameter. Therefore, the color of the mirror changes when the viewing angle changes.
- The shape of the substrate affects the achieved layer thickness. In this case, convex lenses were used and the layer thickness in the center corresponds to the specified one, but at the periphery it decreases. Therefore, a difference is observed between the optical properties of the center and the periphery. This is a disadvantage of the technology and can be avoided by using flat substrates or another synthesis method.

1.1.1. SUBSTITUTION OF Ti_3O_5 WITH ZrO_2 IN OPTICAL THIN FILM COATINGS

The optical function of the coating is far from the only requirement for its implementation. Even with good optical properties, it may turn out that the mechanical durability of the coating is not satisfactory, or that the production process is hindered for some reason. For example, when using Ti_3O_5 to obtain thin-film optical coatings, a higher power of the electron gun is required, which in thicker layers leads to unwanted heating of the substrates. The Ti_3O_5 material itself requires preliminary melting and degassing within several vacuum processes with gradual filling of the molybdenum crucible. This preparation involves the production equipment. Due to the differences in the CTE of Ti_3O_5 and the substrate, after cooling this leads to cracking of the coating. In addition, the application of Ti_3O_5 is accompanied by the supply of oxygen into the vacuum chamber, which in itself leads to additional requirements and variable factors that can affect production.

The present experimental work considers the replacement of Ti_3O_5 with ZrO_2. Zirconium dioxide is also used in the production of optical thin-film coatings. Its refractive index is slightly lower than that of titanium oxides, but its application does not require oxygen supply and preliminary preparation - ready-to-use tablets are used.

For the purposes of the study, two theoretical coatings with specified optical curves were developed – one based on trititanium pentoxide (coating 1) and the other – on zirconium dioxide. The coatings must meet the requirement for a residual peak of reflectance below 1% and look similar in order to be interchangeable within the manufacturer's catalog – optical curve shape type "W", maximum of reflection in the region $\lambda<490$ nm, minimum at $\lambda = 500$ nm, residual peak at $\lambda = 600$ nm. (Fig. 37).

Coating 1 (Ti_3O_5)	Coating 2 (ZrO_2)
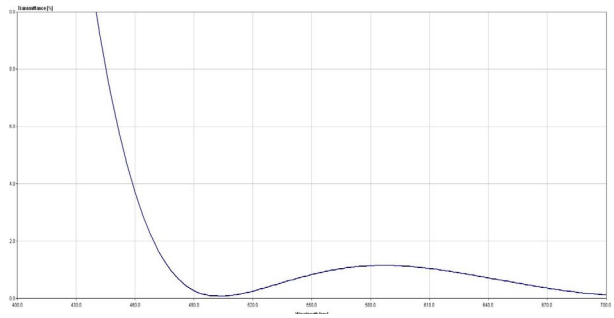	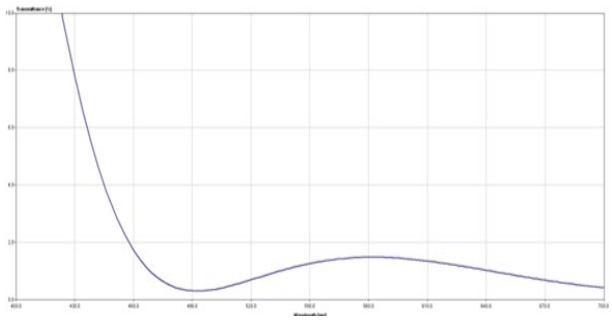

Figure 10. Optical curves of coatings containing Ti and Zr calculated with MCalc.

In industrial conditions, it is good for the anti-reflective coatings to be composed of no more than 6 optically active layers (the vacuum process also includes adhesive, antistatic, hydrophobic layers) in order to maintain good production time. Formulations for coatings made up of 4 active layers have been developed that meet the task and are presented in Table 6.

Table 6. Target thicknesses in the coatings.

Coating 1		Coating 2	
Material	Thickness [nm]	Material	Thickness [nm]
Ti_3O_5	27.93	ZrO_2	30.28
SiO_2	42.29	SiO_2	42.29
Ti_3O_5	40.63	ZrO_2	44.04
SiO_2	120.56	SiO_2	120.56

The coatings were obtained by EBPVD method in the company "DIO" EOOD - Plovdiv and examined with a spectrophotometer. The optical curves of the obtained coatings are presented in Fig. 11 and correspond to the theoretical ones.

Coating 1 (Ti_3O_5)	Coating 2 (ZrO_2)
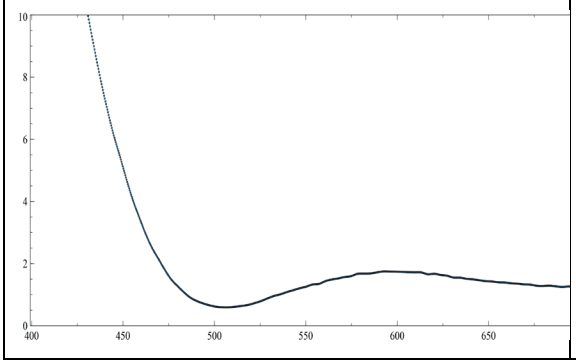	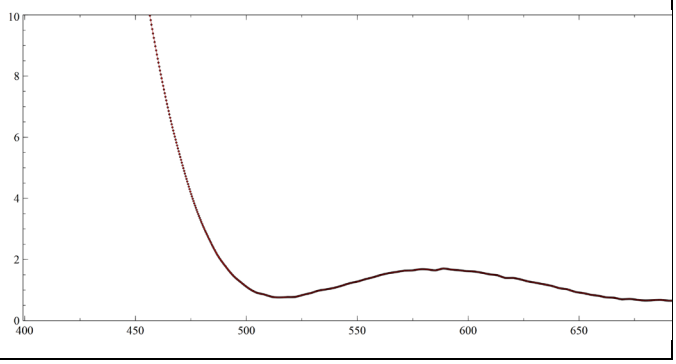

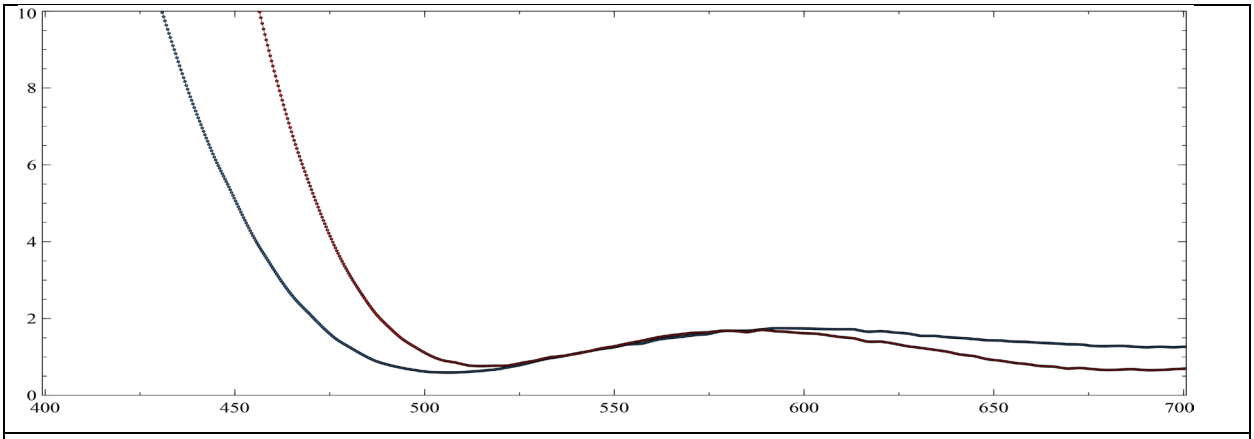

Figure 11. Experimental measurement of the obtained coatings

When comparing the measured curves for the two coatings, horizontal and vertical shifts are observed. The vertical shift is due to the difference in refractive indices between ZnO_2 and Ti_3O_5. It can be compensated by fine-tuning the thicknesses of the coatings. The horizontal shift for the ZrO_2 coating is due to a deviation in the thickness of one of the layers. To eliminate it, the approach from 7.1.3 can be used. – simulation of an optical curve with computational software that contains the deviation and subsequent calibration of the equipment.

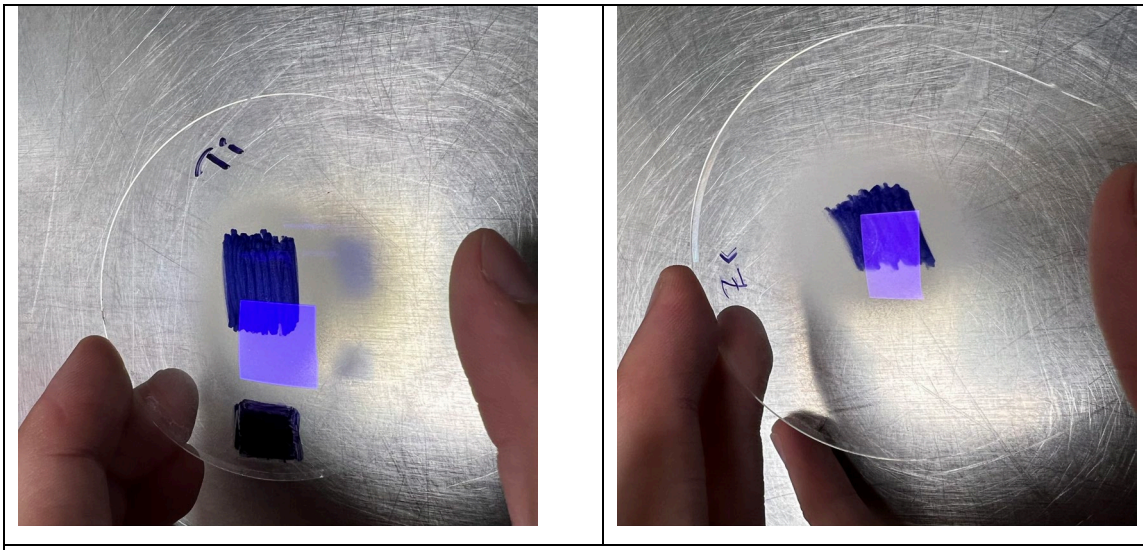

Figure 12. Visual inspection of the obtained coatings.

7.2.SILICONE COATINGS CONTAINING RGO AND ZnO

7.2.1. GO AND RGO SYNTHESIS

A combined method between those proposed by Hammers and Tour was applied to obtain GO. In order to improve the oxidation of graphite, to increase the yield of GO and to improve the

degree of oxidation of graphite, a mixture of concentrated sulfuric and phosphoric acid was used simultaneously, as in the Tour method, and $NaNO_3$ (in the Hammers method, only concentrated sulfuric acid and $NaNO_3$ are introduced). In order to improve the solubility and faster homogenization of the reaction mixture, the addition of potassium permanganate was made in the form of a preheated aqueous solution, instead of a powder. This leads to an increase in the yield of graphite oxide and better exfoliation of the graphite layers, which is proven by XRD.

Flake graphite is ground in a Fritsch high-speed agate ball mill, model Analisette 3 SPARTAN, Pulverisette. The graphite prepared in this way is mixed with sodium nitrate in a ratio of 2:1. Concentrated sulfuric and phosphoric acid (9:1) are added to the resulting mixture, and the components are mixed in an ice bath and under constant intensive stirring with a magnetic stirrer, until complete homogenization for 30 minutes. An aqueous solution of potassium permanganate (the graphite/potassium permanganate ratio is 1:3) is gradually added to the mixture dropwise in an ice bath. Stirring is continued for another two hours with gradual heating to 60-70°C. The resulting mixture is left for 24 hours. Then a 3% aqueous solution of hydrogen peroxide is slowly added dropwise over 1 hour (under a fume hood), with constant stirring.

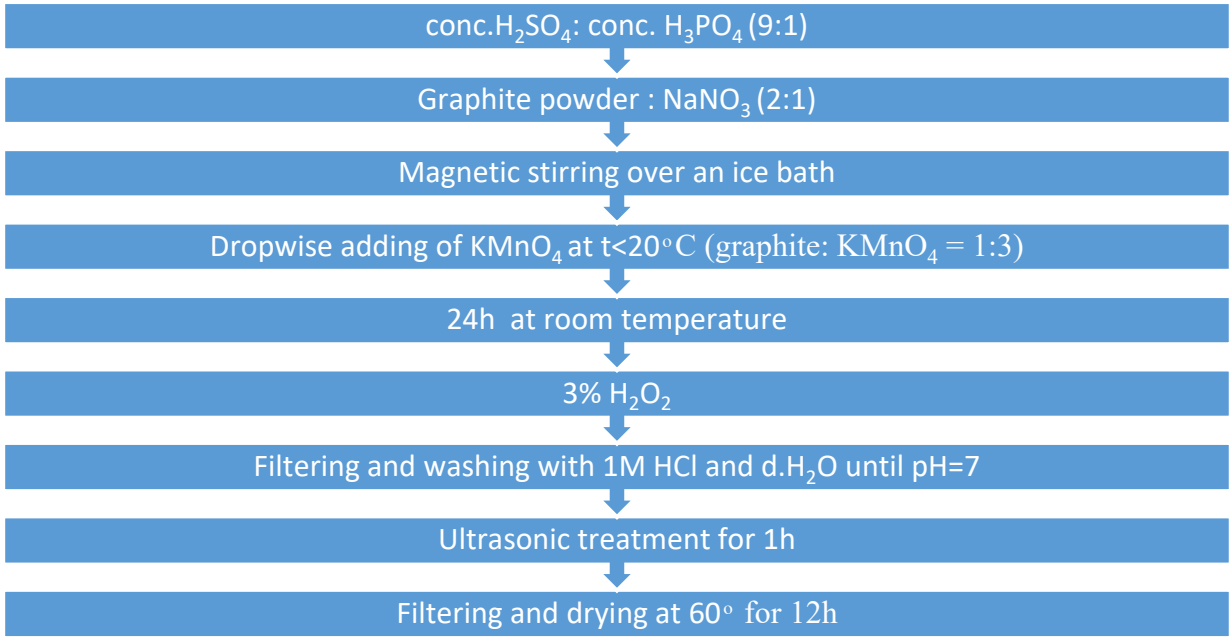

Figure 13. Route of synthesis of GO by modified Hummer's method [84].

After the addition, the mixture is stirred for another 1 hour with a magnetic stirrer. The solution is then filtered using a Buchner funnel and a vacuum pump. To remove metal ion impurities, the resulting precipitate is washed several times with a previously prepared 1M hydrochloric acid solution. This is followed by washing with distilled water to a neutral pH. This is followed by

treatment with an ultrasonic reactor for 1 hour and filtration and repeated washing with ethyl alcohol. The resulting graphene oxide is placed in a dryer for 12 hours at a temperature of 60°C.

The GO obtained in this matter was reduced with ascorbic acid in the dept. of silicate technology in the UCTM:

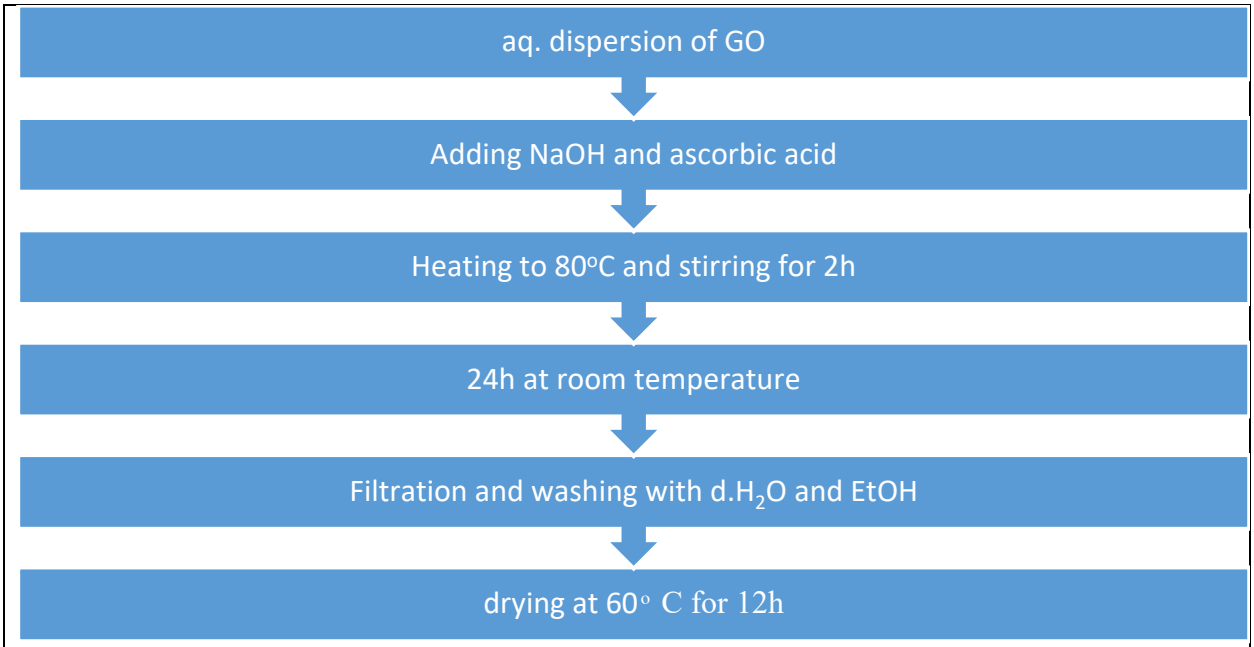

Figure 14. Route for obtaining RGO from GO using L-ascorbic acid as a reducing agent[84].

To the GO suspension already dispersed with the help of ultrasound, we add sodium hydroxide to adjust the pH of the suspension and after its complete dissolution we add a solution of the reducing agent L-Ascorbic acid ($C_6H_8O_6$). Stirring is continued, with gradual heating to 80°C and stirring for 2 h. After the time has elapsed, the solution is left to stand for 24 h at room temperature. This is followed by filtration with a Buchner funnel under vacuum and drying of the resulting reduced graphene oxide (RGO) for 12 h at 60°C.

7.2.2. NANOSIZED ZnO SYNTHESIS

The required amount of zinc acetate dihydrate is weighed on a technical scale and ground using an agate mortar for 5 minutes. 10 ml of propyl alcohol is added. The resulting suspension is heated in a water bath at 60°C until the zinc acetate dissolves, then acetic acid is added. Stirring with a magnetic stirrer continues until a gel forms, after which the temperature is gradually increased to 100°C and it is dried. The resulting powder is transferred to a crucible and heated in an oven for three hours at 220°C, and then at 420°C for 5 hours.

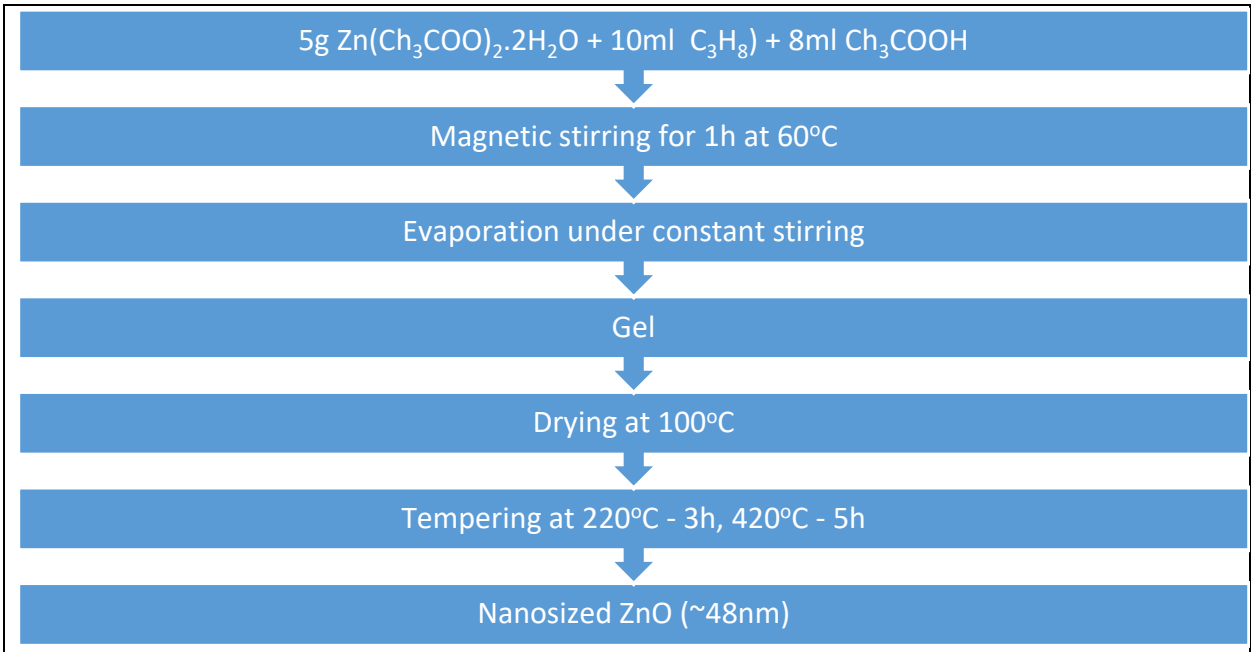

Figure 15. Route for synthesizing nanosized ZnO[83].

7.2.3. OBTAINING SILICONE COMPOSITES

All composite materials were obtained in the dept. of silicate technology at the UCTM:

Table 7. **Compositions of silicone samples**

№	Additives	Additive contents		
1	RGO	1 mass %	3 mass %	5 mass %
2	GO	1 mass %	3 mass %	5 mass %
3	ZnO	1 mass %	3 mass %	5 mass %
4	ZnO + 5 % RGO	1 mass %	3 mass %	5 mass %

Silicone rubber was purchased from Shin-Etsu Chemical Co., Ltd. The technical sheet is presented in table 8. Silicone is offered in a two-component form, which polymerizes when mixed.

Table 8. Technilca sheet of silicone rubber					
№	Test items	Unit	Test Result	Specifications	Test Method
1	Appearance A side	*	Translucent	Translucent	Visual
2	Viscosity RV-1 at 23° C Shear rate 0.9 s^{-1}	Pa.s	1010	700 – 1500	JIS Z 8803
3	Viscosity RV-1 at 23 °C Shear rate 10 s^{-1}	Pa.s	416	100 - 800	JIS Z 8803
4	Curing Time: T10; MDR at 130 °C	Sec	23	15 – 30	Rotorless Rheometer
5	Curing Time: T90; MDR at 130 °C	sec	47	60 max.	Rotorless Rheometer
6	Density : 23° C	g/cm^3	1.13	1.11 – 1.15	JIS K 6249
7	Hardness ; Type A	*	42	35 – 45	JIS K 6249
8	Tensile Strength	MPa	10.0	7.0 – 14.0	JIS K 6249
9	Elongation at Break	%	720	500 – 1200	JIS K 6249
10	Tear Strength :Crescent	kN/m	40	25 – 60	JIS K 6249
11	Weight loss at 200 C x 4 hrs	%	0.34	0.44 max	Heat loss

Equal amounts of silicone components A and B (0.500g each) are weighed, adding silicone oil (about 5 drops) for better homogenization. Each starting component is weighed according to the different compositions and homogenized in an agate mortar. Then, the corresponding amount of the starting component is added to the silicone and mechanically homogenized until good dispersion of the nanoparticles in the silicone matrix is obtained. A layer of each composition is applied to glass substrates, then placed in a dryer at a temperature of 140°C for about 1 minute until complete polymerization of the silicone rubber is achieved. The obtained samples are subjected to structural and phase characterization by SEM, TEM and X-ray phase analysis. Their antibacterial properties are also determined.

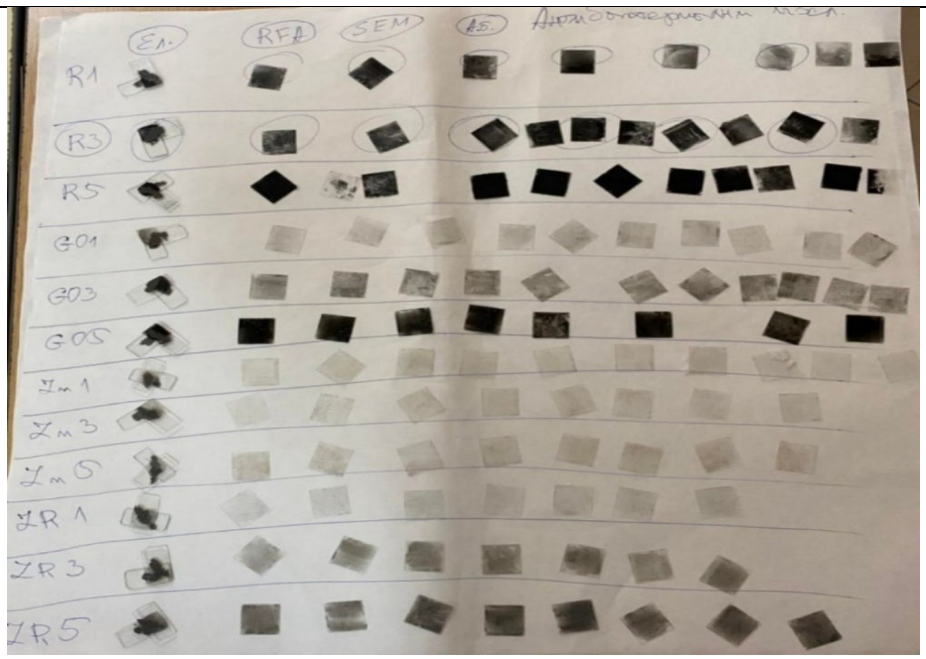

Figure 16. Samples applied to glass substrates.

Determination of antibacterial properties of the resulting silicone composites

Agar disk diffusion testing was developed in 1940. It is the official method used in many clinical microbiology laboratories for routine antimicrobial susceptibility testing. Although not all bacteria can be tested exactly by this method, standardization has been made for testing some pathogens such as streptococci, *Haemophilus influenzae*, *Haemophilus parainfluenzae*, *Neisseria gonorrhoeae* and *Neisseria meningitidis*, using specific culture media, different incubation conditions and different approaches to establish zones of inhibition.

In this method, agar is inoculated with a standardized inoculum of the tested microorganism. Then, filter paper disks (in our experiment, instead of disks, square plates with a diameter of 5 mm) containing the test compound at the desired concentration are placed on the agar surface. The plates are incubated under appropriate conditions. In general, the antimicrobial agent diffuses into the agar and inhibits the growth of the test microorganism. After 24-48 hours, the diameters of the zones of growth inhibition, if any, are measured.

The disk diffusion method is not suitable for determining the minimum inhibitory concentration (MIC), since it is not possible to accurately determine the amount of antimicrobial agent diffused into the agar medium. Nevertheless, an approximate value can be calculated for some microorganisms and antibiotics by comparing the zones of inhibition.

However, the disk diffusion assay offers many advantages over other methods: it does not require special equipment, is cost-effective, can test a large number of microorganisms and antimicrobial agents, and the results obtained are easy to interpret. In addition, some studies have demonstrated great success in patients suffering from bacterial infection and undergoing antibiotic therapy based on the antibiogram of the causative agent. This fact is due to the good correlation between the in vitro data and the development of the disease in vivo.

All obtained silicone composites with the participation of graphene oxide, reduced graphene oxide and zinc oxide, synthesized according to the synthesis scheme in the Experimental Part were studied.

The structure of the obtained silicone composites with the participation of GO, RGO, ZnO and ZnO/(5%RGO) and the interaction between them and the silicone rubber matrix were analyzed by X-ray diffraction using Bruker D8 Advance with LynxEye detector from Bruker using Cu (Ka) radiation at the Institute of Optical Materials and Technologiesat the Bulgarian Academy of Sciences.

The microheterogeneity, the degree of crystallinity and the size of the crystallites of the synthesized materials and composites were determined by scanning electron microscopy (HR STEM JEOL JEM 2100). All SEM images were obtained in the SEM analysis laboratory of the Institute of Optical Materials and Technologiesat the Bulgarian Academy of Sciences.

X-ray diffracion analysis

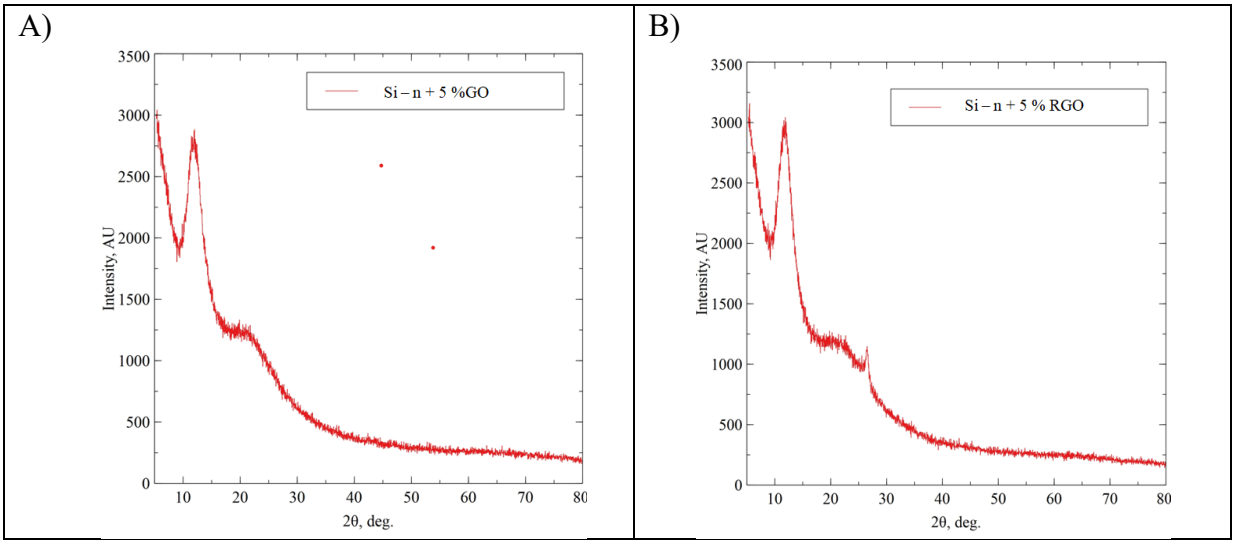

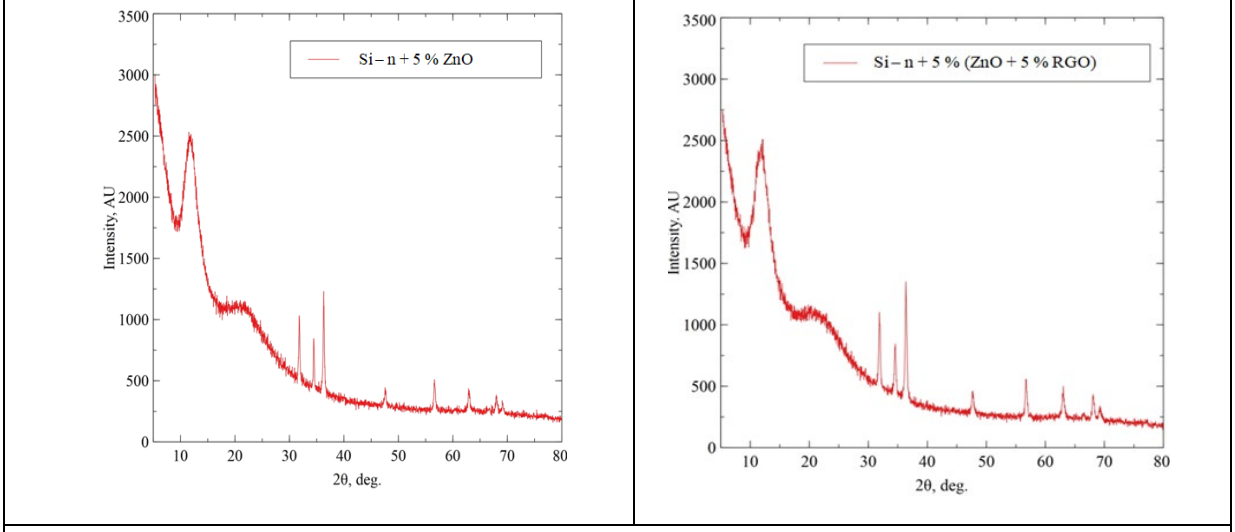

Figure 17. XRD of silicone composites

Fig.17 presents the X-ray diffraction patterns of all obtained silicone compositesIt is evident that silicoone rubber is present in all samples with characteristic peaks at about 12 and 19 degree 2θ. All X-ray diffraction patterns were further processed with QualX 2.0. After reading the peaks and comparing them with an X-ray database, the presence of the corresponding phases in the different composite compositions was proven (Figure 18).

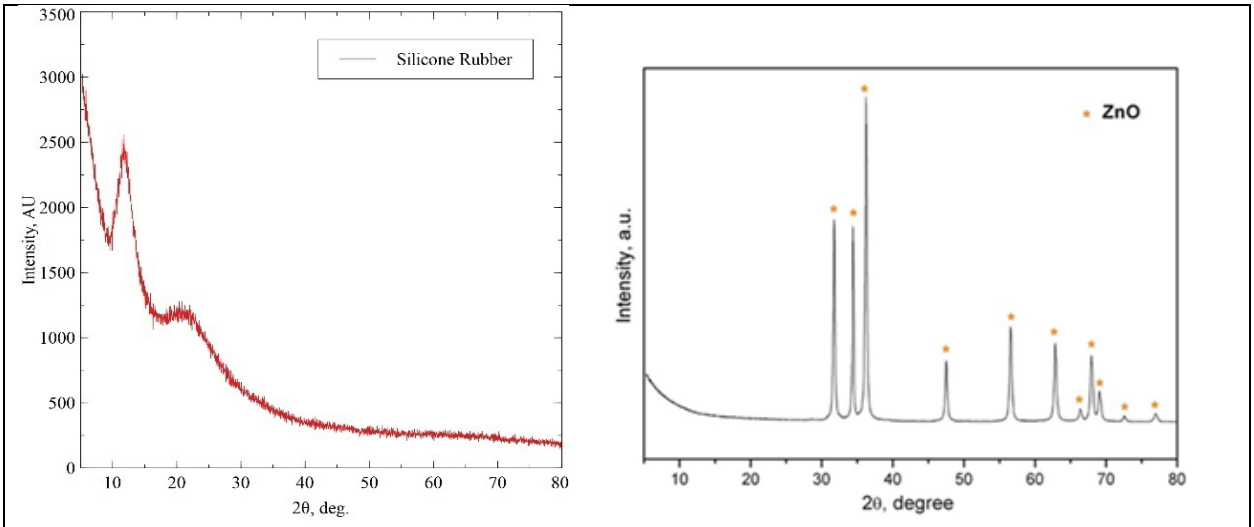

Figure 18.X-ray diffraction patterns of silicone rubber with ZnO NPs.

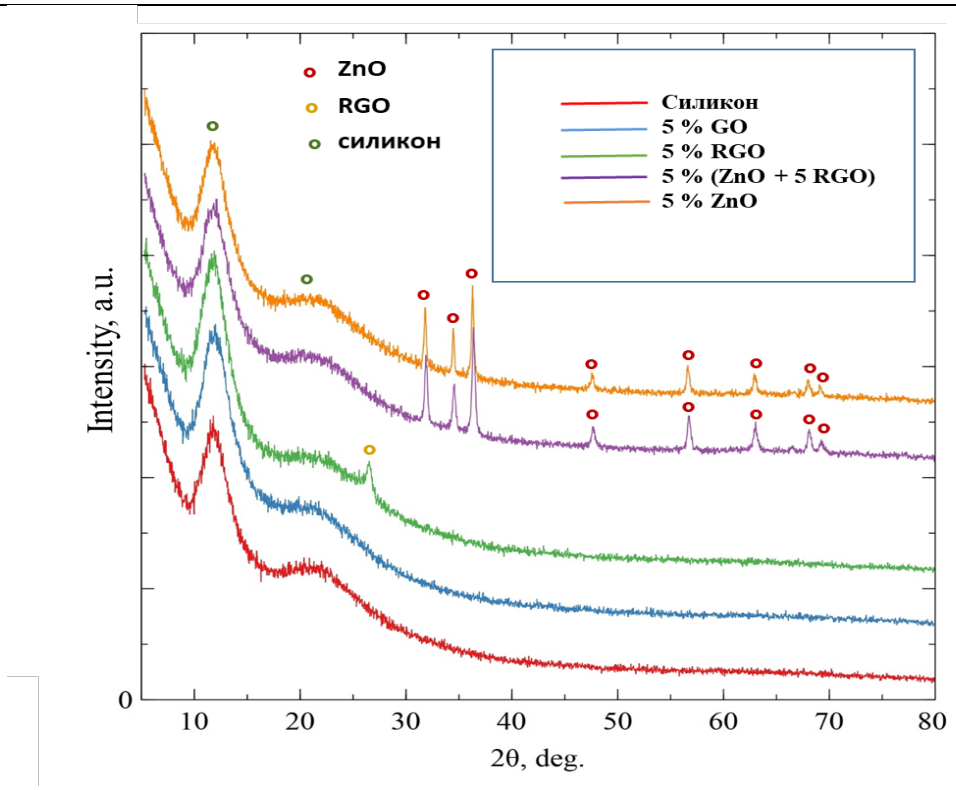

Figure 19. XRD of all compositions.

Fig. 19 presents the X-ray diffraction patterns of the starting silicone rubber and the ZnO nanoparticles synthesized by us, which were used to obtain the silicone composites. The presented X-ray diffraction pattern of ZnO shows that there is a complete ovedrlap of the diffraction maxima with the literature data from X-ray card No. [00-036-1451]. The preparation of a monophasic product from ZnO is proven.

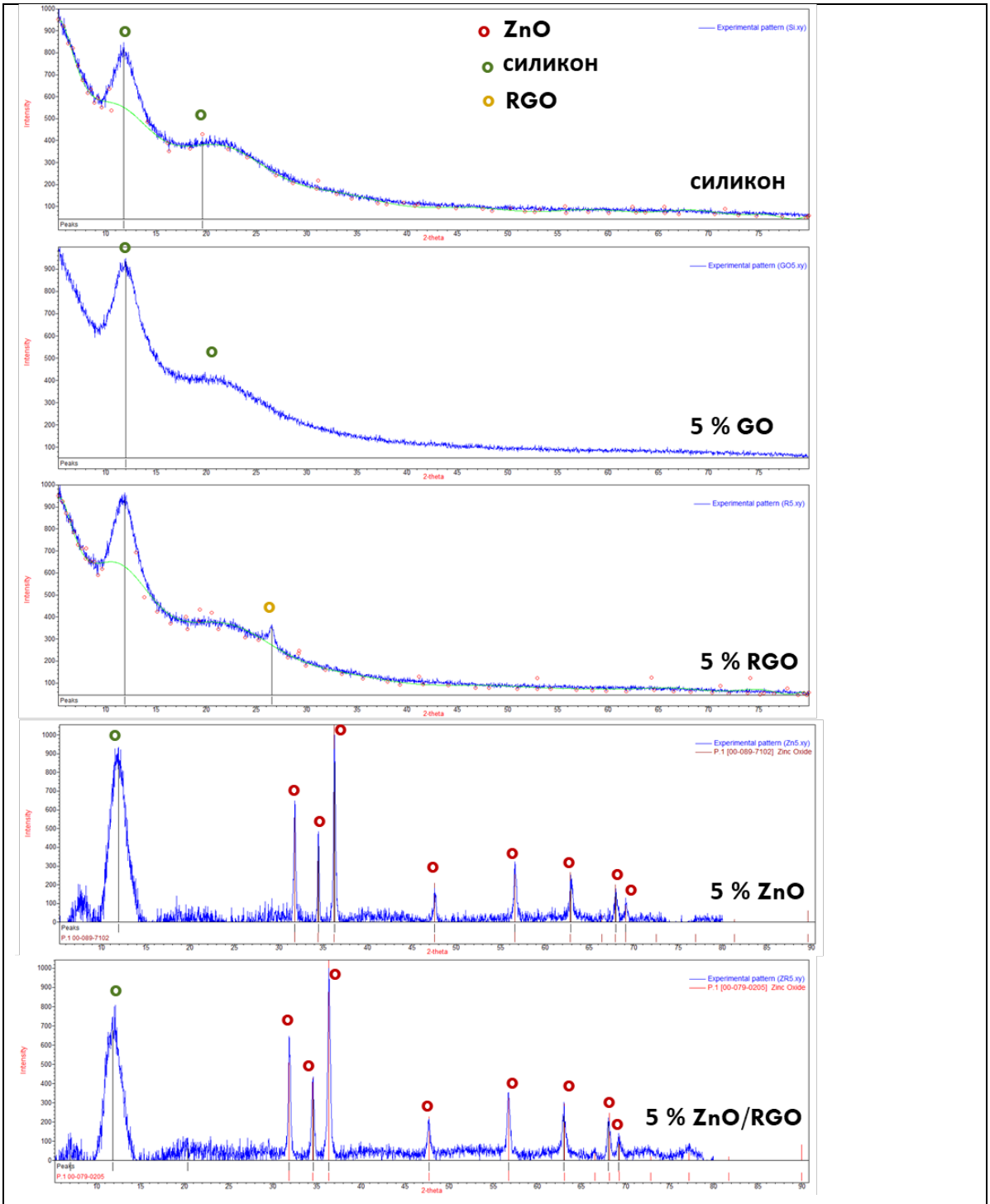

Figure 20. XRD patterns after analysis with QualX2.0.

Fig. 20 presents all the X-ray diffraction patterns of the silicone composites processed and normalized with the QualX program (Altomare et al., 2015). This is a program for qualitative phase analysis using powder diffraction data[96]. QualX is able to perform phase identification by querying a PDF-2 database and with open access: POW_COD. POW_COD was developed by the authors of the QualX program and was created using the structure information contained in the Crystallography Open Database (COD). The PDF database is maintained and continuously

updated by the International Center for Diffraction Data (ICDD) (ICDD, 2003). The main novelty of QualX, with respect to its previously distributed version, is the ability to manage the POW_COD database.

With the help of this program, the size of the ZnO nanoparticles present in the ZR5 and Zn5 silicone composites was determined and averaged over all peaks in the range of 18-28 nm.

ZR5 - silicone composite with 5% [ZnO/(5%)RGO]

In the plane 101 (2θ=36.3) – 28 nm, (this is a 100% characteristic peak). On the other plane - 100 (2θ=31.8) the size is 30 nm. On 002 (2θ=34.5) and 110 (2θ=56.6) it turns out 27 nm. That is, for the size of ZnO in this sample the average size on all peaks is 28nm.

Zn5 - силиконов композит с 5 % ZnO

In the plane 101 (2θ =36.3) – 18 nm, (100% characteristic peak). Plane 100 (2θ=31.8) reveals a size of 19 nm. At planes 002 (2θ=34.5) and 110 (2θ=56.6) we calculate 18 nm. Averaging all sizes, for ZnO in this sample we assube a size of 18 nm.

SEM analysis

Fig. 21 presents SEM images of the obtained silicone composites. From the SEM images it was possible to draw some conclusions about the overall incorporation and distribution of the graphene structures in the silicone matrix. Agglomerates of ZnO and RGO are observed, distributed over the compact structure of the silicone. These images do not give a clear idea of the microstructure and distribution of the ZnO nanoparticles in the silicone matrix, since the smooth silicone surface is mainly observed.

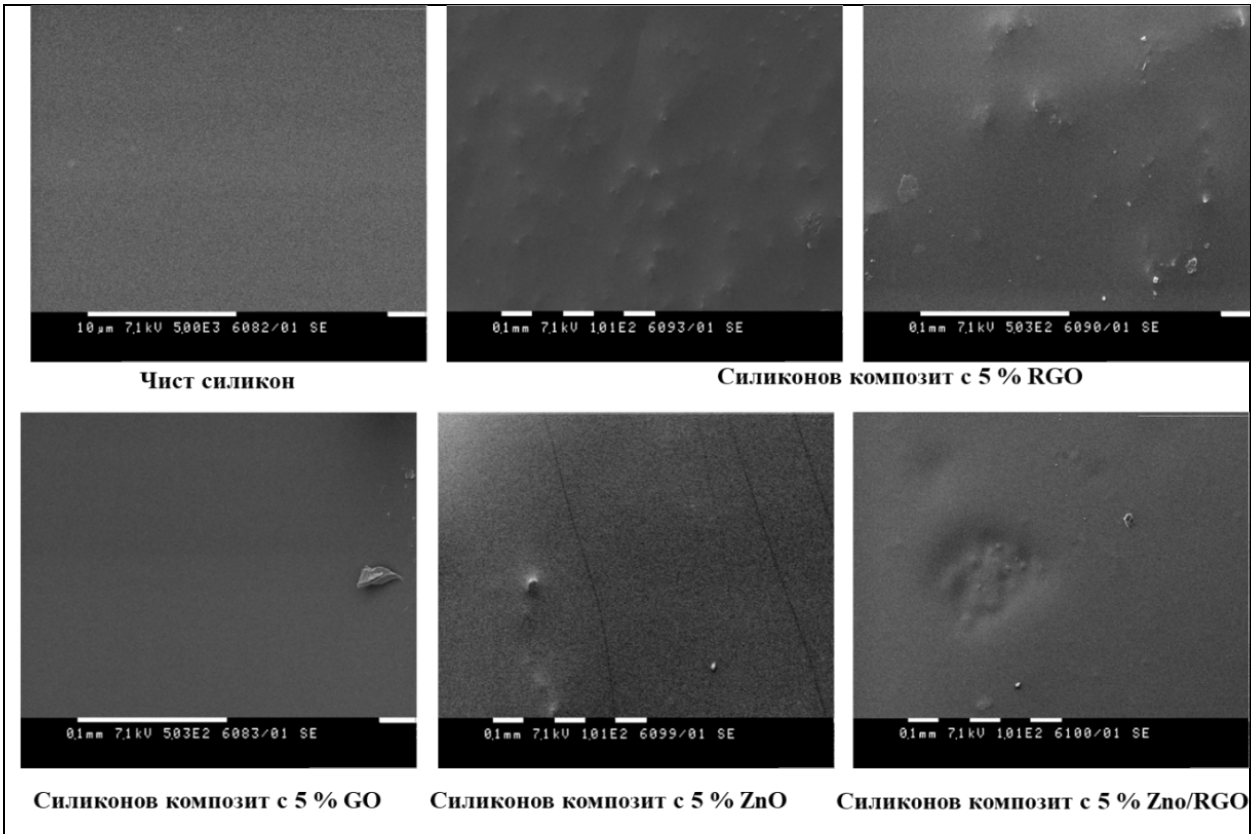

Фиг. 21. SEM images of silicone rubber and the obtained composites.

Transmission electron microscopy (TEM)

In order to more clearly observe the distribution and microstructure of the obtained silicone composites, TEM analysis was performed.

The obtained TEM images of a silicone composite with 5% RGO at different magnifications are presented in Fig. 22. At magnifications of 6,000 x and 10,000 x, thin, silky, transparent formations characteristic of graphene structures are clearly observed. At magnifications of 40,000 x, folded carbon sheets located in the silicone matrix are visible.

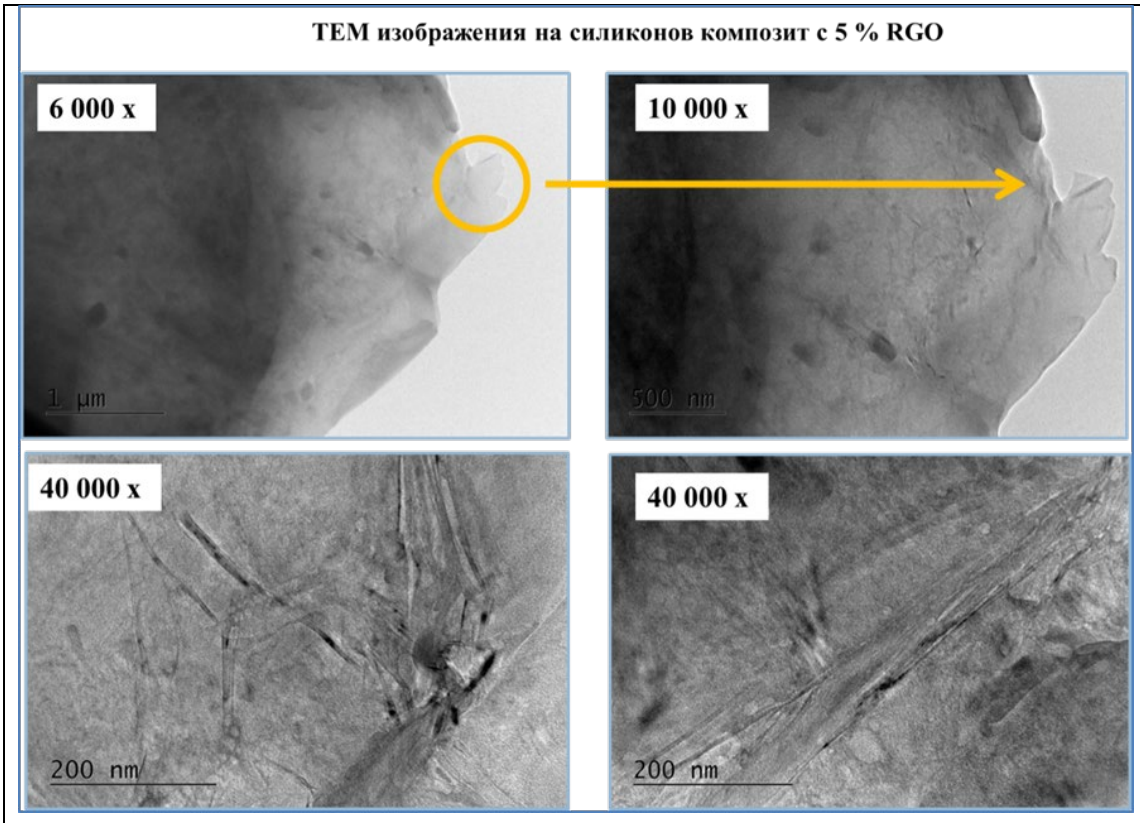

Figure 22. TEM of silicone composite with 5 % RGO at different magnifications

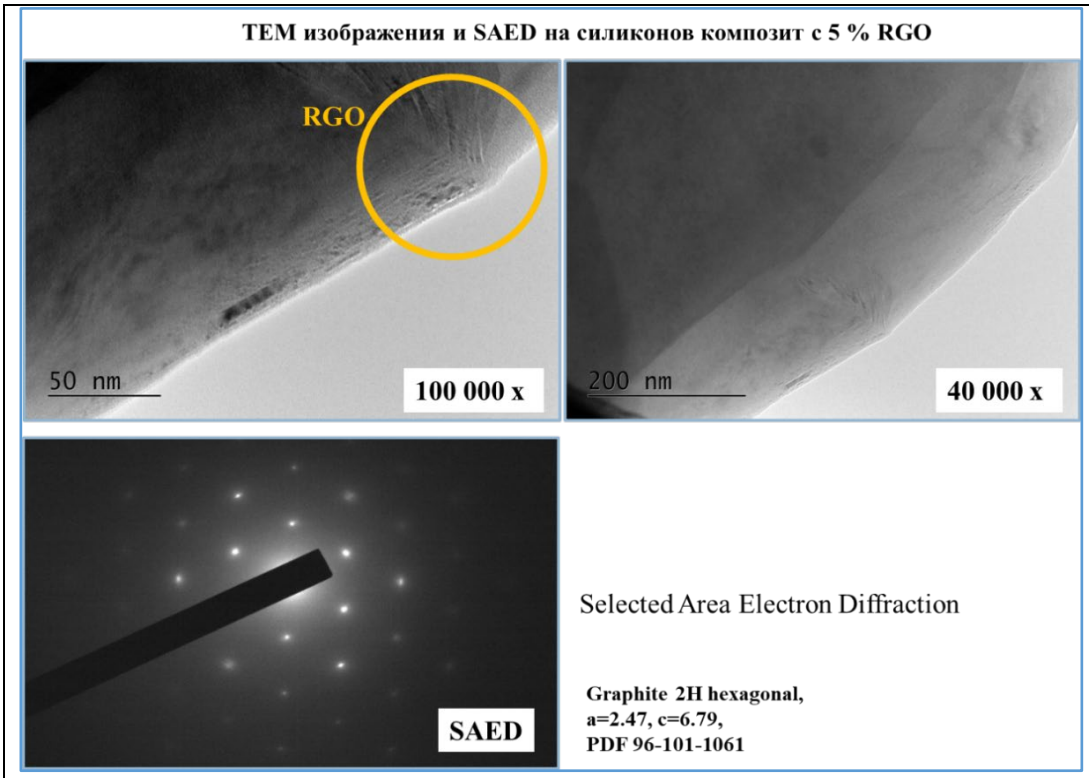

Figure 23. TEM images with SAED (Selected Area Electron Diffraction) of silicone composite with 5% RGO at different magnifications

In Fig. 23 at a magnification of 100,000x, the well-separated layers of RGO in the silicone matrix are observed. From the diffraction study conducted in the selected area electron diffraction (SAED) mode of a silicone composite with 5% RGO, a conclusion was made about the structure of the carbon single layer and the parameters of the crystal lattice were determined - Graphite 2H hexagonal, a=2.47, c=6.79, PDF 96-101-1061.

In Fig. 24 at 40,000x magnification, elongated ZnO nanocrystals are observed, located in the silicone matrix. From the study conducted by selected area electron diffraction (SAED) of a silicone composite with 5% ZnO, a conclusion was made about the structure of the ZnO nanocrystallites and the crystal lattice parameters were determined - Zincite hexagonal, a= 3.24900 Å, c= 5.20700 Å, # 96-901-1663).

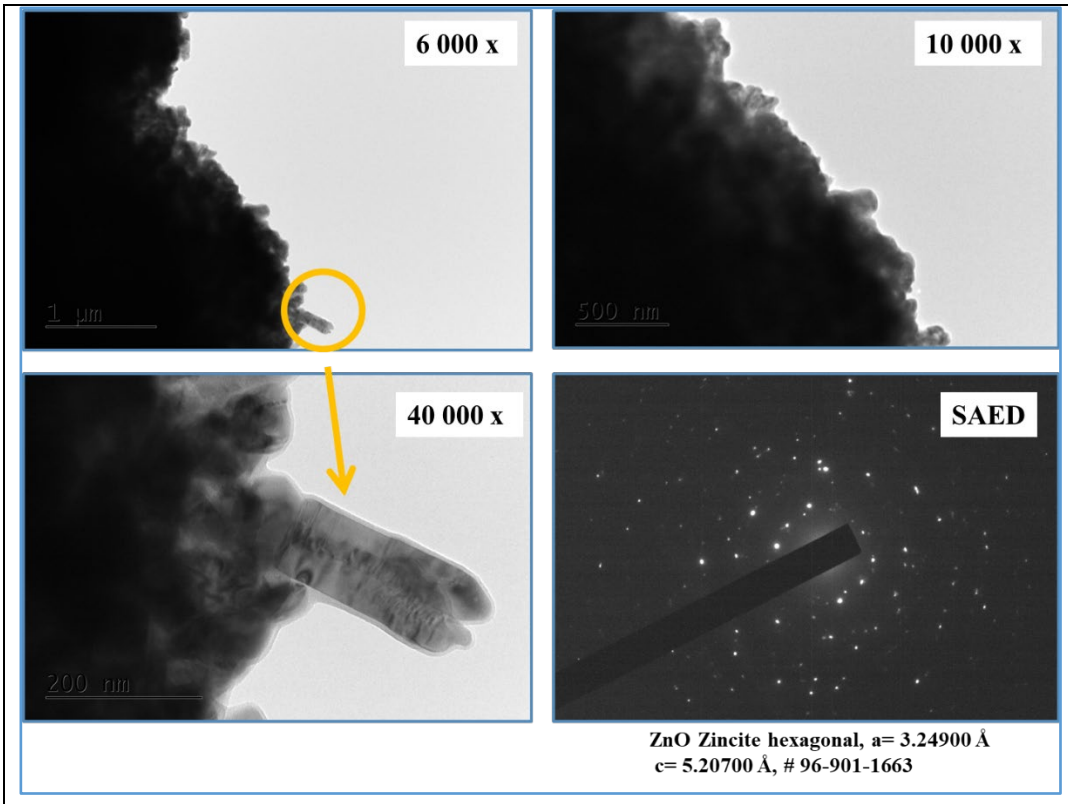

Figure 24. TEM images and SAED (Selected Area Electron Diffraction) of a silicone composite with 5% ZnO at different magnifications.

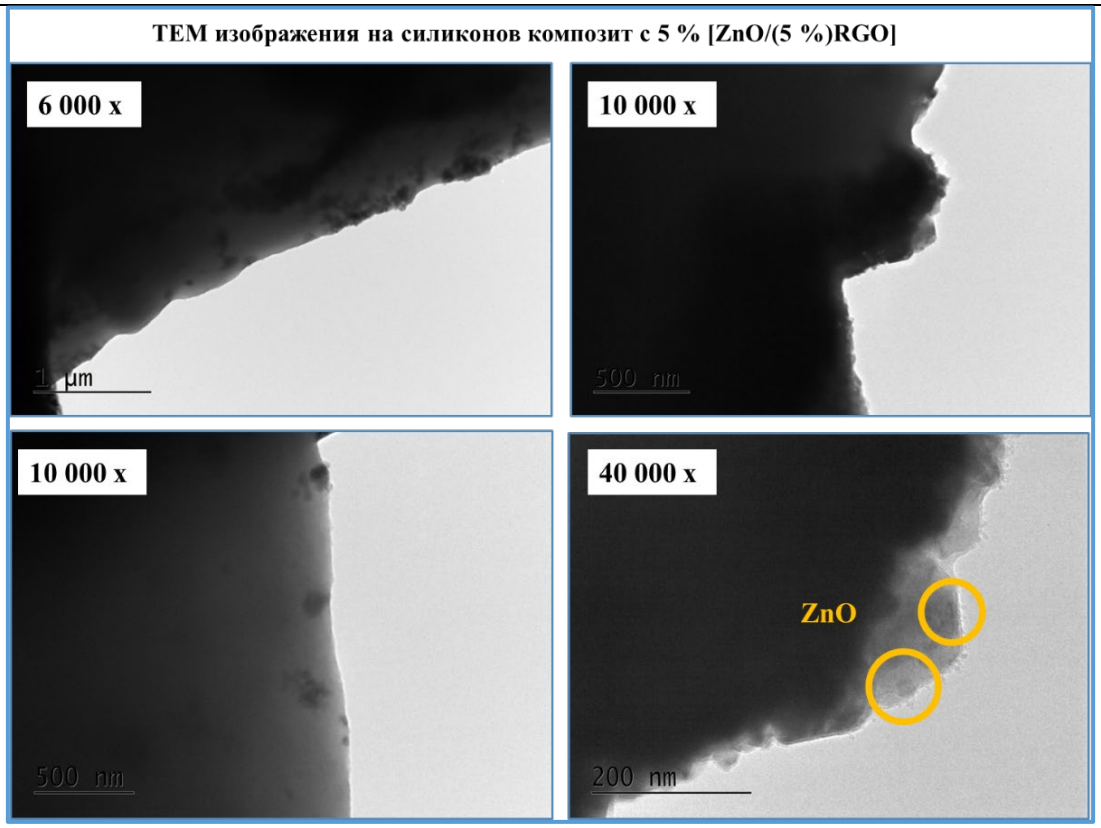

Figure 25. ТЕМ изображенияна силиконов композит с 5 % [ZnO/(5%)RGO] при различни увеличения.

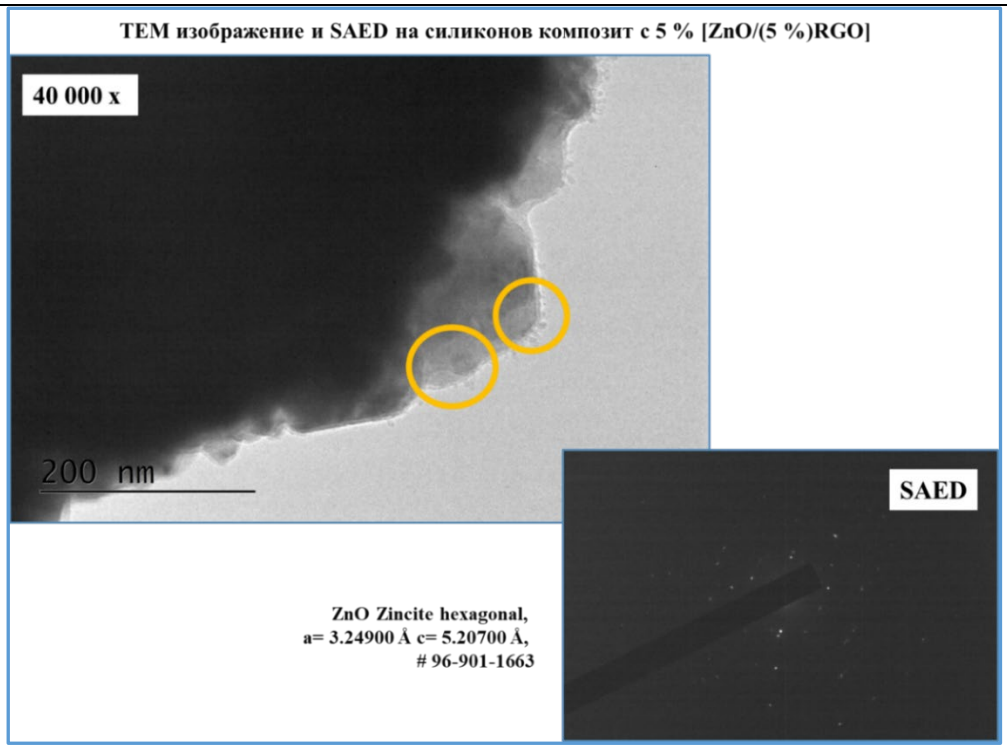

Figure 26. ТЕМ изображения и SAED (Selected Area Electron Diffraction) на силиконов композит с 5 % [ZnO/(5 %)RGO] при увеличение 40 000x.

In Fig. 25 and 26, at magnifications of 10,000 and 40,000 times, well-formed ZnO nanocrystals are observed, located in the silicon matrix.

From the study conducted by selected area electron diffraction (SAED) of a silicon composite with 5% [ZnO/(5%)RGO], a conclusion was made about the structure of the ZnO nanocrystallites and the parameters of the crystal lattice (Zincite hexagonal, a= 3.24900 Å, c= 5.20700 Å, # 96-901-1663).

Assessment of the antibacterial effect of the obtained nanocomposites

Table 9. Antibacterial activity against *Escherichia coli* and *Staphylococcus aureus.*

№	Състав на нанокомпозитите, *%*	***Escherichia coli***	***Staphylococcus aureus***
1	1 mass % GO + Si – n (GO1)	No sterile zones	No sterile zones
2	3 mass % GO + Si – n (GO3)	No sterile zones	**Contact inhibition**
3	5 mass % GO + Si - n (GO5)	No sterile zones	No sterile zones
4	1 mass % RGO + Si - n (R1)	No sterile zones	No sterile zones
5	3 mass % RGO + Si - n (R3)	No sterile zones	No sterile zones
6	5 mass % RGO + Si - n (R5)	No sterile zones	No sterile zones
7	1 mass % ZnO + Si - n (Zn1)	No sterile zones	**Contact killing**
8	3 mass % ZnO + Si-n (Zn3)	No sterile zones	No sterile zones
9	5 mass % ZnO + Si - n (Zn5)	No sterile zones	No sterile zones
10	1 mass % ZnO/5 %RGO + Si – n (ZR1)	No sterile zones	**Contact killing**
11	3 mass % ZnO/5 %RGO + Si - n (ZR3)	No sterile zones	**Contact killing**
12	5 mass % ZnO/5 %RGO + Si - n (ZR5)	No sterile zones	No sterile zones
13	Si (A+B)	**Contact inhibition**	**Contact killing**

Table 9 presents data from studies conducted on the antibacterial activity of the obtained silicone composites against *Escherichia coli* and *Staphylococcus aureus.*

In the agar diffusion method used by us to determine the antibacterial activity of the obtained silicone composites, the agar is inoculated with a standardized inoculum of the tested

microorganism. Then, square glass plates with the applied silicone composite measuring 5x5 mm are placed on the agar surface. The Petri dishes are incubated under appropriate conditions. The tested agent diffuses into the agar and affects the growth of the tested microorganism for 24 h, and then the diameters of the growth inhibition zones, if any, are measured. In this method, the material is allowed to diffuse onto a solid, inoculated culture medium. If the substance being analyzed has a bacteriostatic or bactericidal effect, a zone of inhibition is recorded. The size of the zone of inhibition is a function of the concentration and certain physicochemical properties of the substance being analyzed.

In the majority of the samples examined, no sterile zone was observed (Fig. 27-31), which is due to the method used and the type of samples, which are solid and cannot diffuse into the agar. In a silicone composite with a composition of 3% GO (GO3), contact inhibition against the bacteria Staphylococcus aureus was observed (Fig. 31). And contact killing against the bacteria Staphylococcus aureus was established in the silicone composites with a composition of 1 mass % ZnO (Zn1), 1 mass % ZnO/5 %RGO (ZR1), 3 mass % ZnO/5 %RGO (ZR3).

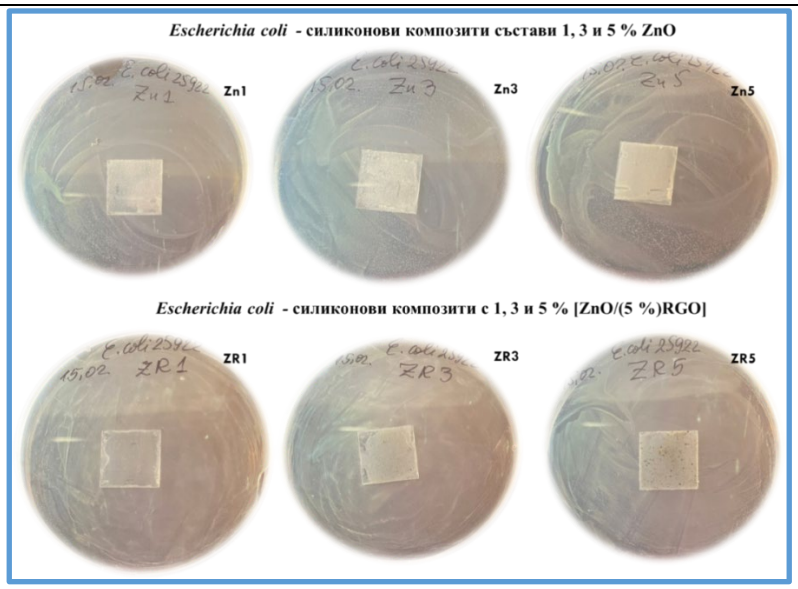

Figure 27. Petris of composites with ZnO and RGO [ZnO/(5 %)RGO], *Escherichia coli*.

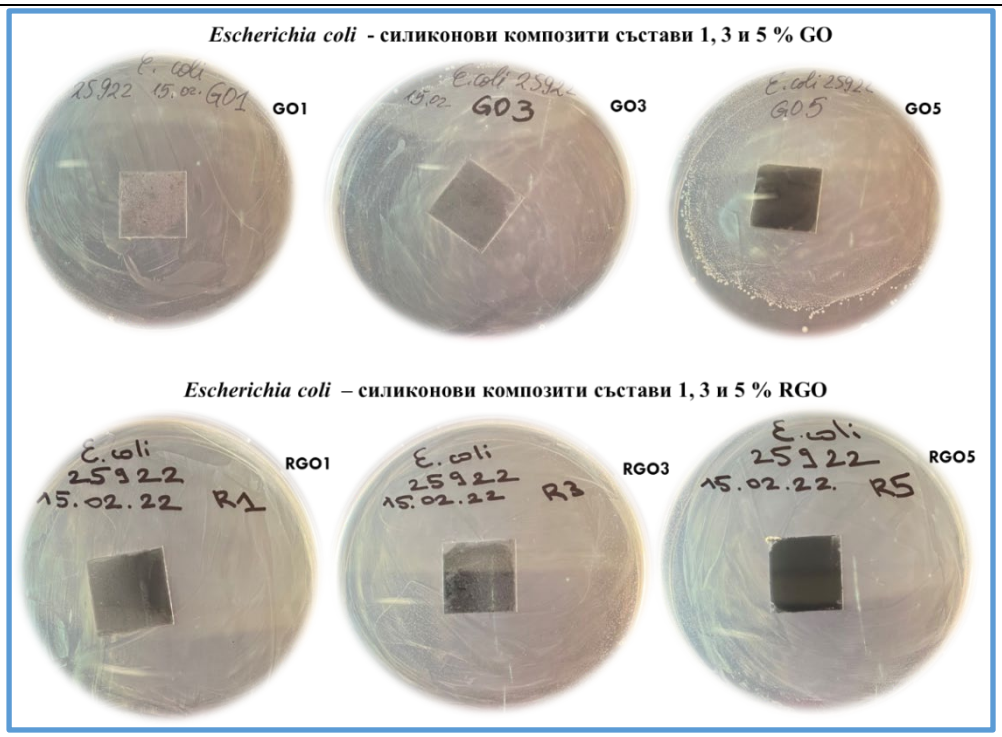

Figure 28. Petris with composites with GO and RGO, *Escherichia coli*.

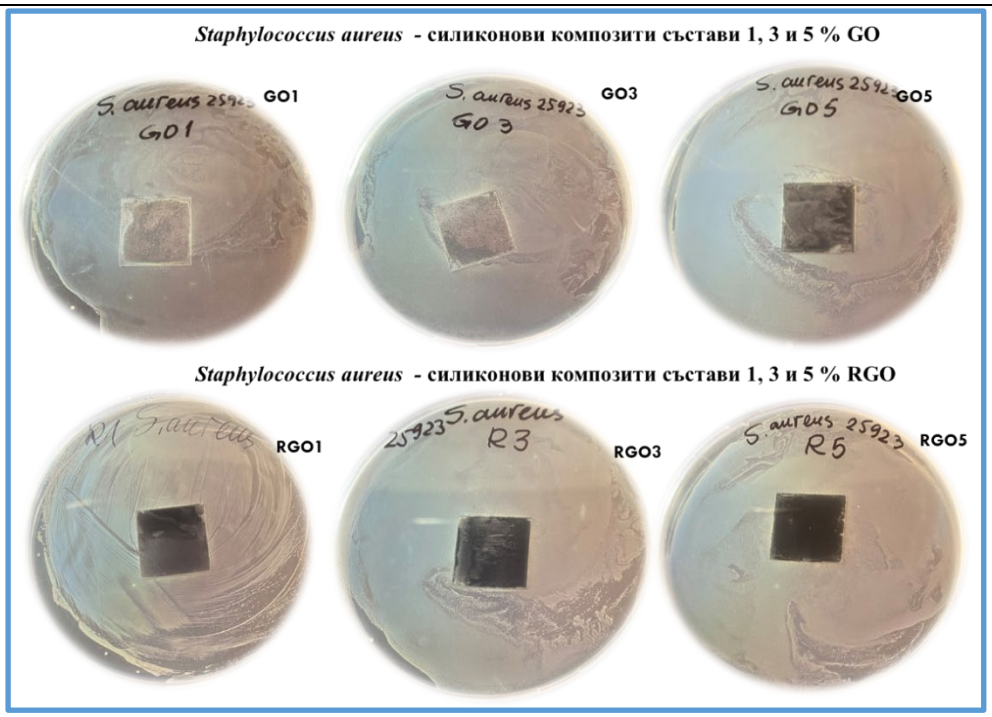

Figure 29. Petris with GO and RGO, *Staphylococcus aureus.*

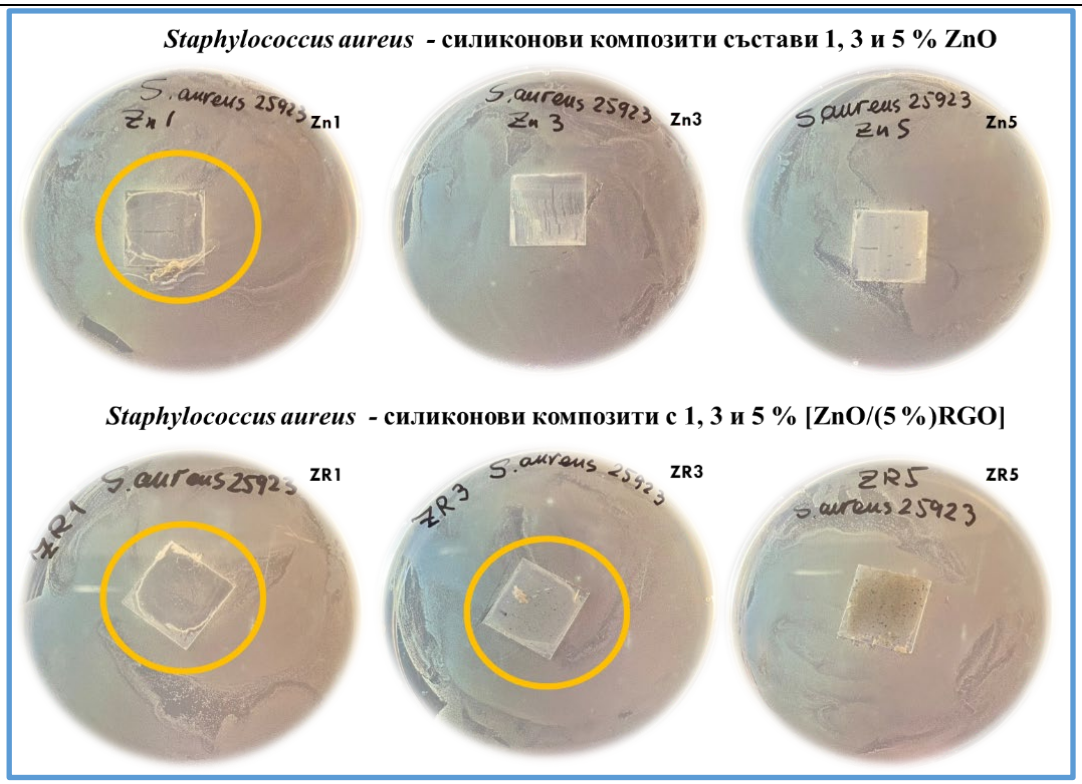

Figure 30. Petris with ZnO and [ZnO/(5 %)RGO], *Staphylococcus aureus.*

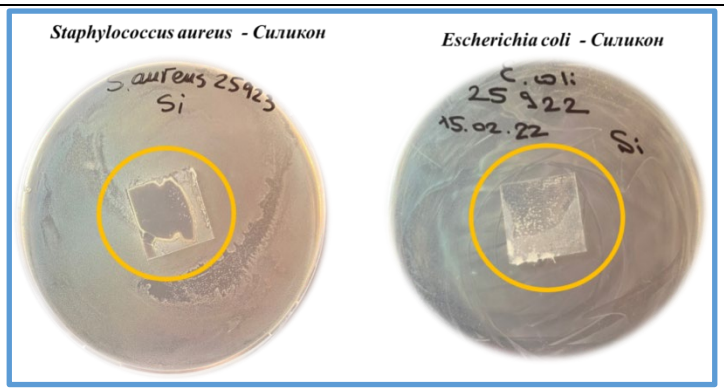

Figure 31. Petris with unmodified silicone, *Escherichia coli* and *Staphylococcus aureus.*

It should be noted that pure silicone rubber showed contact killing and, accordingly, contact inhibition against both bacteria Staphylococcus aureus and Escherichia coli (Fig. 59).

The convenience of the agar diffusion method used by us lies in the rapid results, which allow it to be used as a screening method for the presence or absence of antibacterial effect of the studied nanomaterials. Additional studies are pending, including dynamics.

7.3.EPOXY COATINGS WITH GPL. EFFECT OF MATRIX VISCOSITY ON GPL LAYER DISPERSION AND DELAMMINATION.

Dispersion and delamination of GPL layers remains a key challenge to obtain isotropic properties of coatings. By using higher or lower concentrations of the precursors BPA and ECH, the viscosity of the suspension can be influenced. With its increase, more limited sedimentation and a higher concentration of GPL particles in the suspension are expected.

For the purposes of the study, suspensions of GPL in methanol were prepared by sonication. The suspensions thus obtained were added to BADGE-precursor with different amounts of vaporizer and applied as coatings by dip coating. Due to the volatility of the solvents, the amount of dry mass after polymerization of the epoxy was calculated using the formula:$M\% = \frac{M_C}{M_M}.100\%$

whereas:
M% - calculated amount of dry matter (polymerized epoxy resin)
M_c – sample weight after polymerization and drying
M_M – sample weight before polymerization and drying

Table 10. Mass percent concentration of dry matter after polymerization.

Sample	Mass. %
Control	31.6 %
T0	32.3 %
T1	34.5 %
T2	36.7 %

The control sample contains the factory-prepared precursor and does not un dergo further modification and the addition of additives. In sample T0, the polymer matrix is unmodified, but the GPL suspension is added. T1 and T2 are subjected to stirring with heating to 40ºC for 8 and 16h, respectively, to remove part of the volatile fraction, thus increasing the viscosity and dry concentration.

A working suspension of 0.128g GPL in 50ml methanol is prepared in a beaker. The suspension is sonicated for 15min at an amplitude of 30%, maximum permissible probe temperature 70ºC. 3ml of the working suspension is added to samples 1., 2., and 3. under constant stirring with a magnetic stirrer. The coatings are applied by dip coating on glass substrates, which are subjected to polymerization at 100ºC for 1 hour.

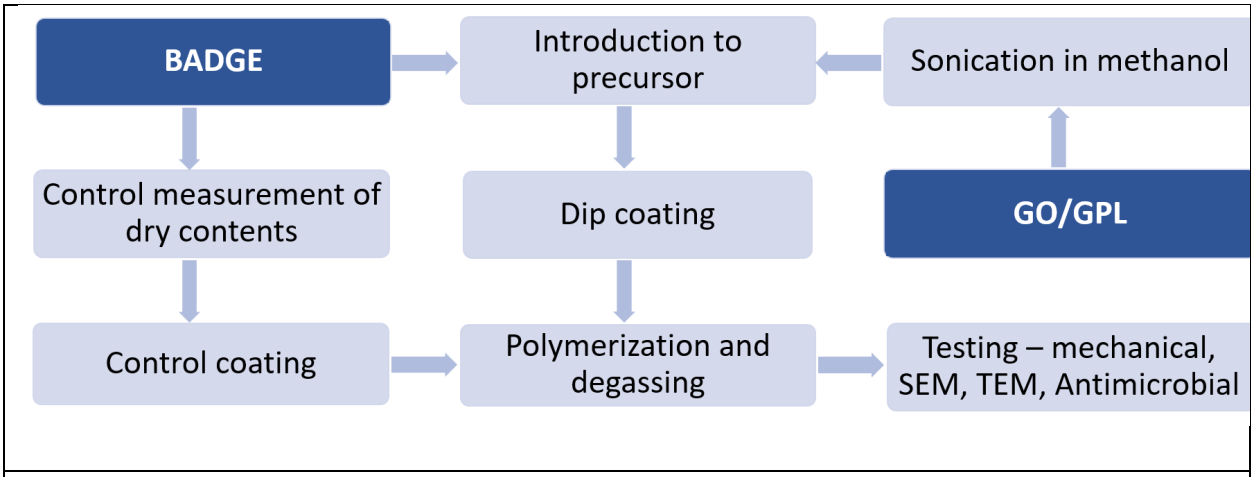

Figure 32. Route of preparation of the coatings

To obtain information on the morphology and dispersion of GPL in the polymer composites, samples T0, T1 and T2 were examined by TEM. Selected area electron diffraction (SAED) was also performed to characterize the crystallographic structural data.

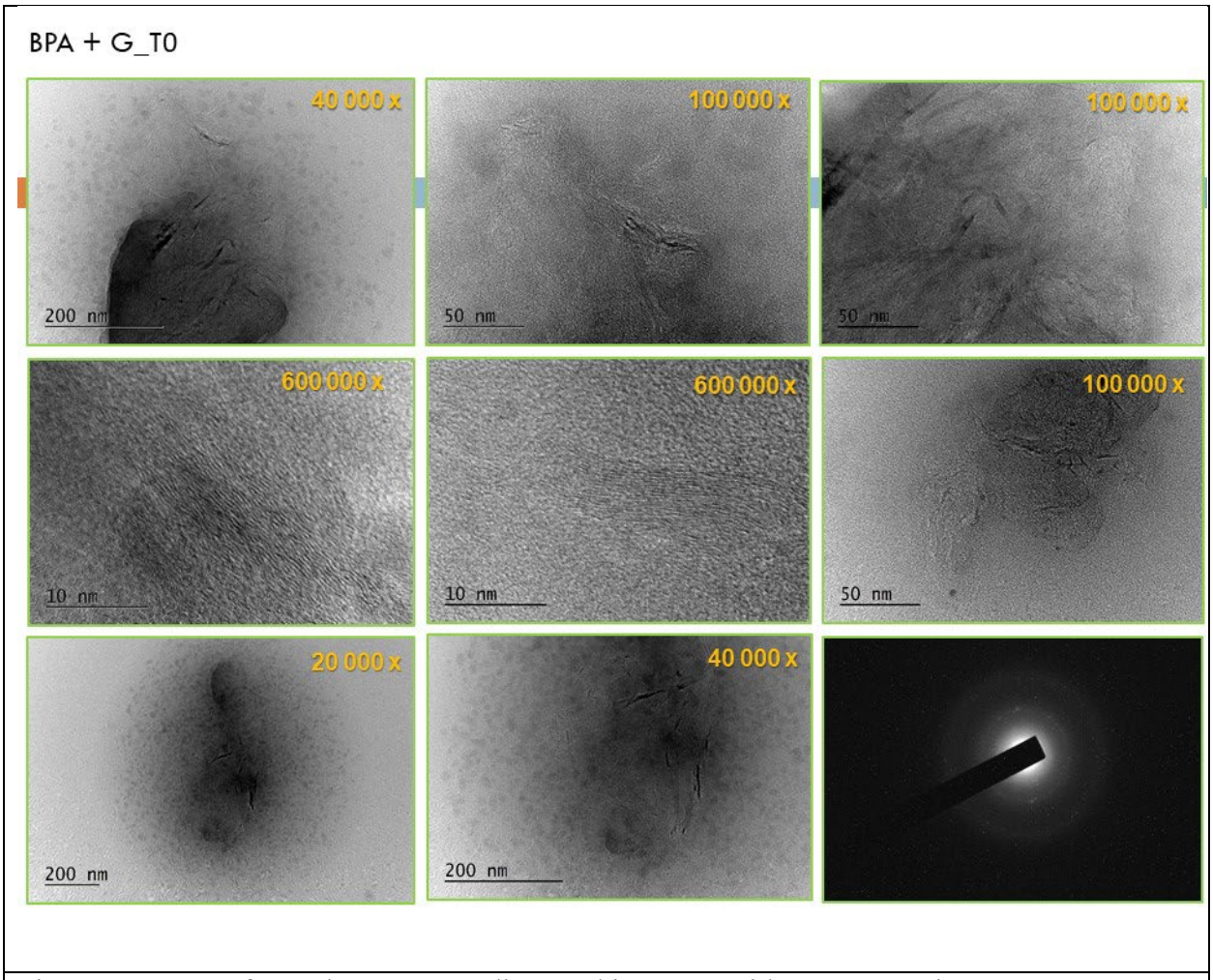

Figure 33. TEM of sample T0 – GPL dispersed in epoxy with no evaporation.

In Fig. 33. we observe partial preservation of the delamination of graphene sheets in the composition of GPL. Agglomeration of the layers into macrostructures is observed, but the integrity of the layers is well preserved. From SAED, in addition to an amorphous halo, we also observe weak reflexes that point to a graphite structure – the delamination is incomplete. Additional literature review and additional experiments are needed.

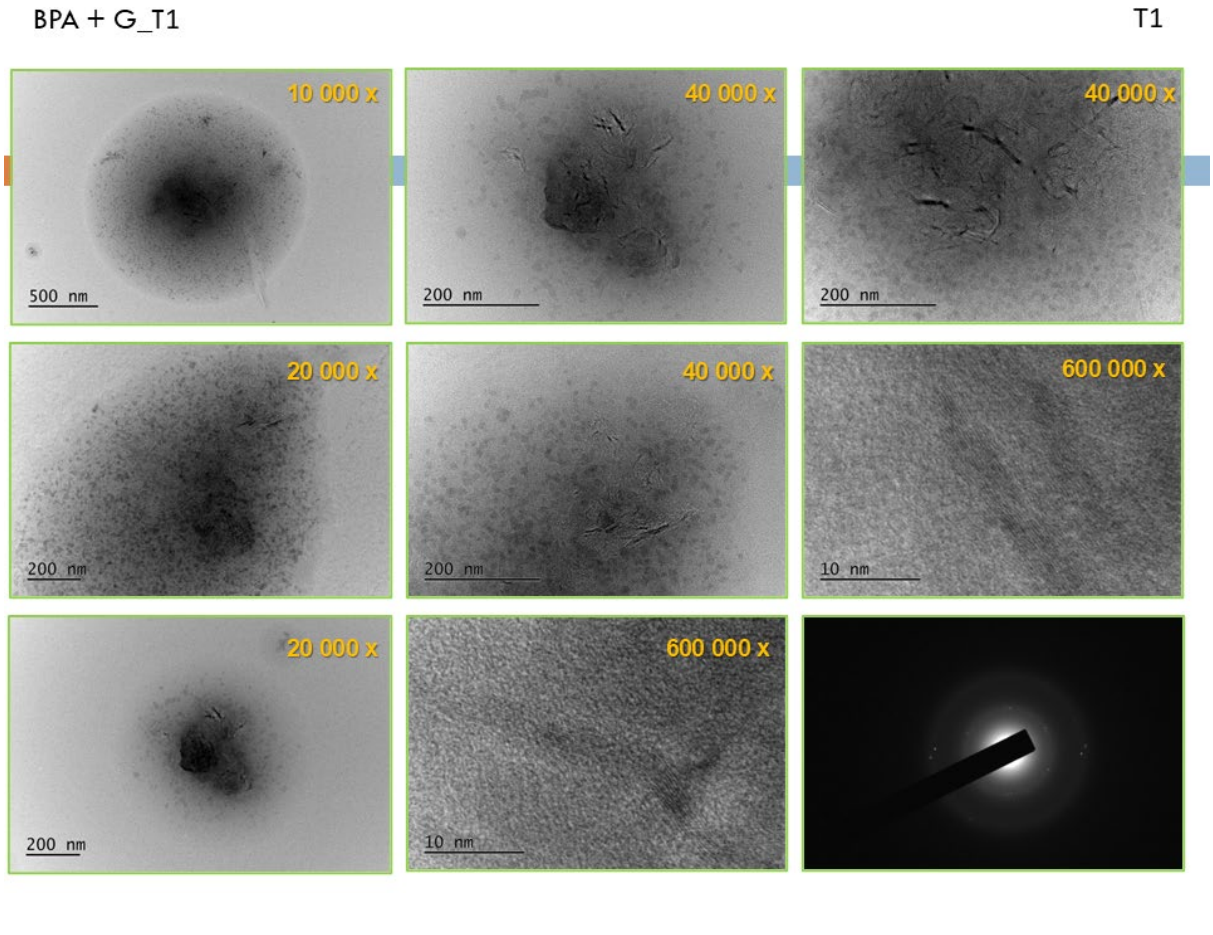

Figure 34. TEM of sample T1 – GPL dispersed in epoxy with 8h evaporation.

Sample T1 shows folded sheets with initiated fragmentation and a high degree of association between nanoparticles with some degree of stabilization at a certain distance. SAED shows weak reflections pointing to a hexagonal structure, but the signal is too weak.

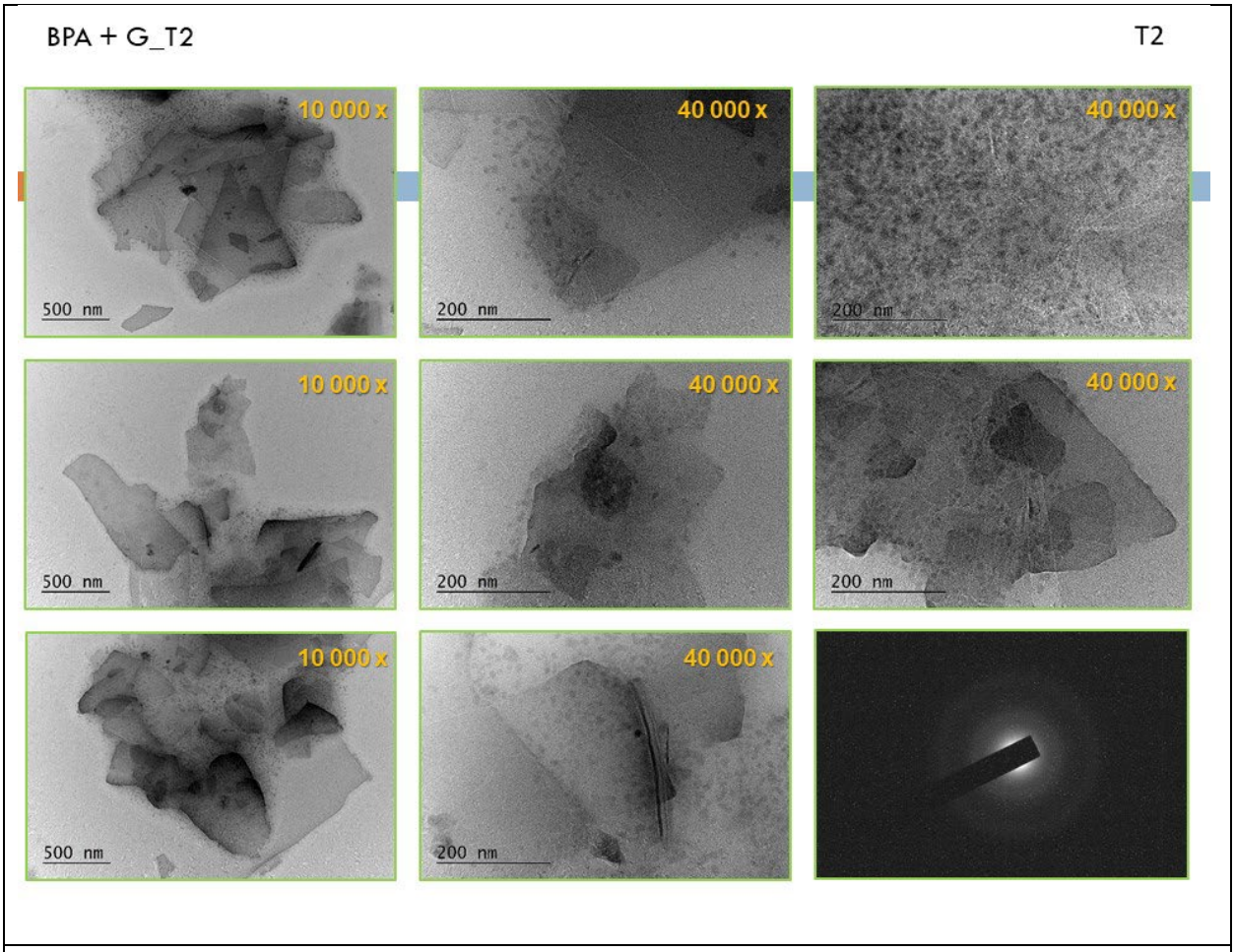

Figure 35. TEM of sample T2 – GPL dispersed in epoxy with 16h evaporation.

From Fig. 35. it is seen that in the composition of the polymer with the highest concentration of precursors T2, the lamination of the graphene layers is the best. Clearly delaminated single layers are observed, at the expense of violating the integrity of the sheets. The amorphous halo in SAED does not show any reflexes, which is in accordance with the expectations in the presence of well-delaminated graphene layers.

The results confirm the working hypothesis that the higher viscosity of the polymer matrix helps to stabilize the graphene layers and prevents their aggregation.

Raman Spectroscopy Results

The analysis was performed with a RENISHAW inVia Raman microscope with a microscope model: inVia Qontor Microscope with Leica objectives, and a CCD detector at a room temperature of 21° C. The apparatus was calibrated with a silicon standard and a peak was obtained at 521 cm-1. Each sample was placed on a glass substrate (2mm), scanned for 30 s, in 5 repetitions, using Wire 5.6 software. A laser with a wavelength of 532 nm and an output power of 50 mW was used

for excitation. The nominal power used in the analysis was 5 mW in accordance with the concentration in the sample under study. In order to focus the laser beam and collect the scattered light in a backscattering configuration, an X50 objective was used. The diameter of the illuminated spot on the sample surface was about 1 μm. The studied spectral range is 10.00 cm-1 – 3500.00 cm-1.

The obtained data were processed with Origin 2024. Fig. 36 shows the initial data plotted. Even at first glance, the shape of the curves shows that no shifts are observed, but there are differences in the intensities and the ratio between the intensities of the obtained peaks.

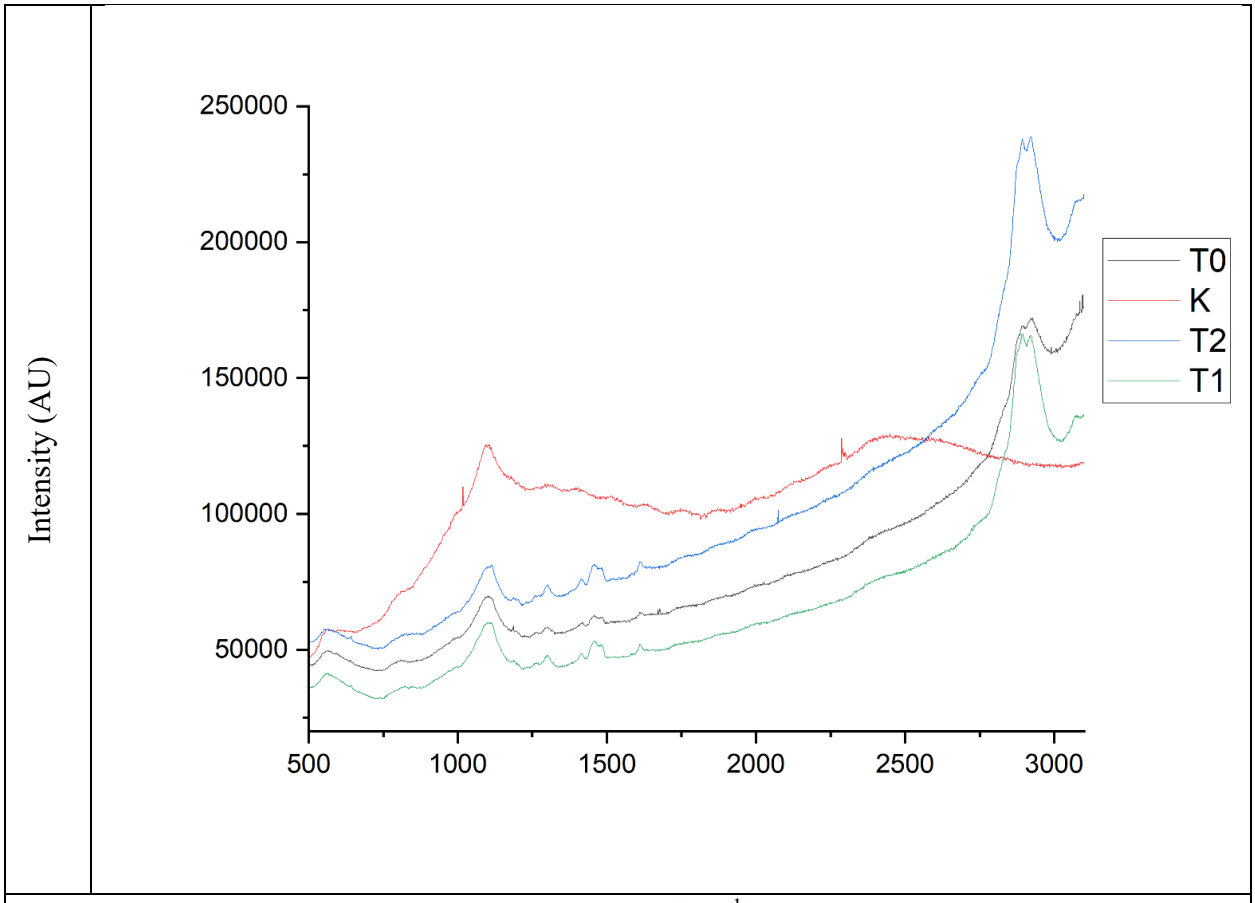

Figure 36. Raman shift of samples K, T0, T1 and T2 before signal processing.

The control sample as well as the other samples show a peak at 1100cm^{-1}, which we attribute to the polymer matrix. In the samples with GPL additives, peaks appear at around 1300, 1456, 1600 and 2900cm^{-1}, which are of interest for the measurement.

At the next stage of the analysis, a least squares method was applied to remove background noise. The processed data are positive, so the asymmetry factor was set to 0. The obtained function was subtracted from the experimental data and a smoother curve was obtained – the minima are referred

to the same value. Since the intensity is in relative units, its absolute value does not bring us analytical information – we factor the graphs to base zero Fig. 37.

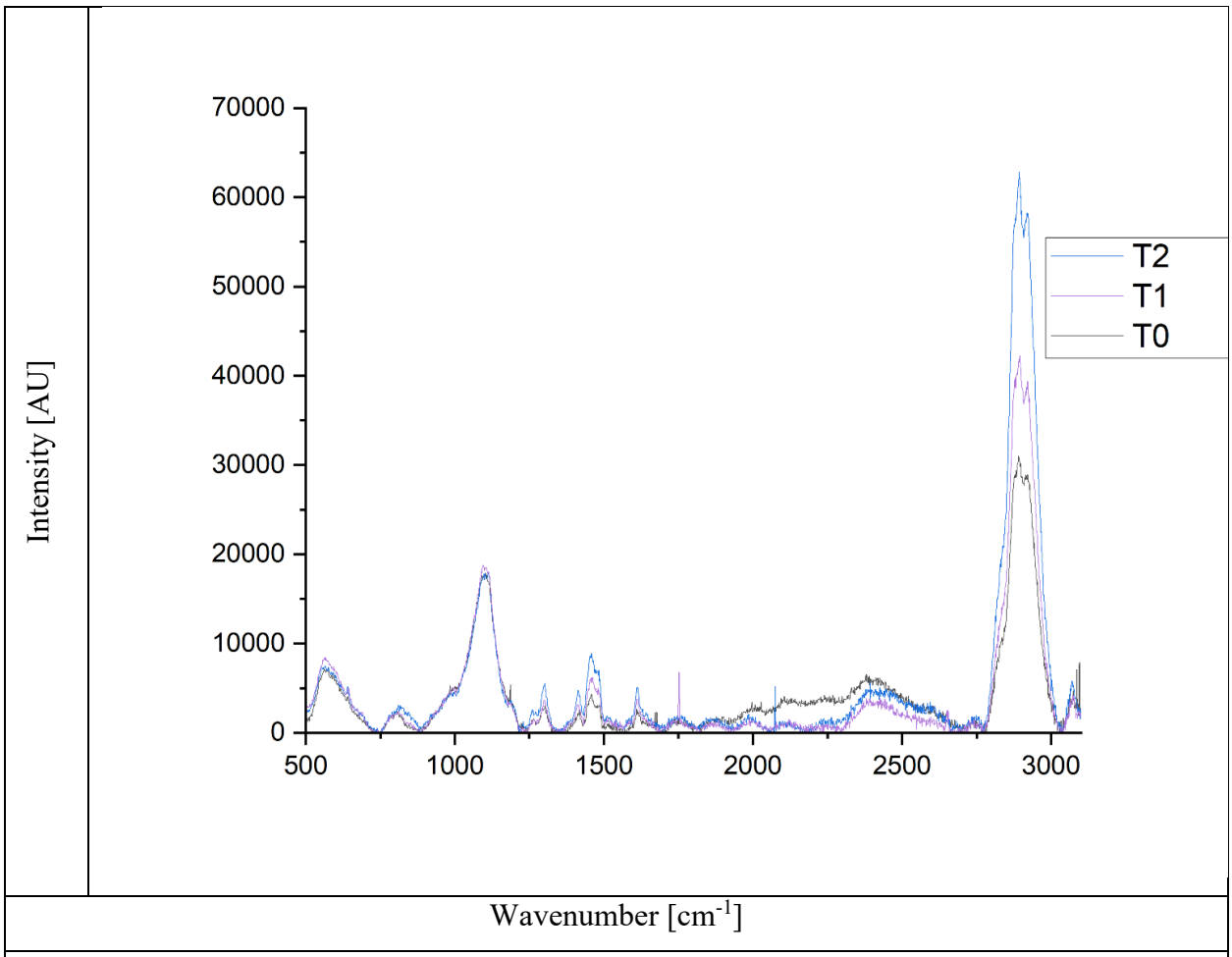

Figure 37. Raman shift of samples K, T0, T1 and T2 after background noise subtraction.

In this form, the data show a regular increase in the intensity of both the 2D and G bands with the order of the sample. Although the ratio between the 2D/G band also increases, it would be premature to draw a conclusion about a change in the number of layers in the sample. The proposed hypothesis is about an increase in the concentration of the non-precipitated GPL in the suspension, which remained bound in the coating.

For greater clarity, the data are compared together in Fig. 38.

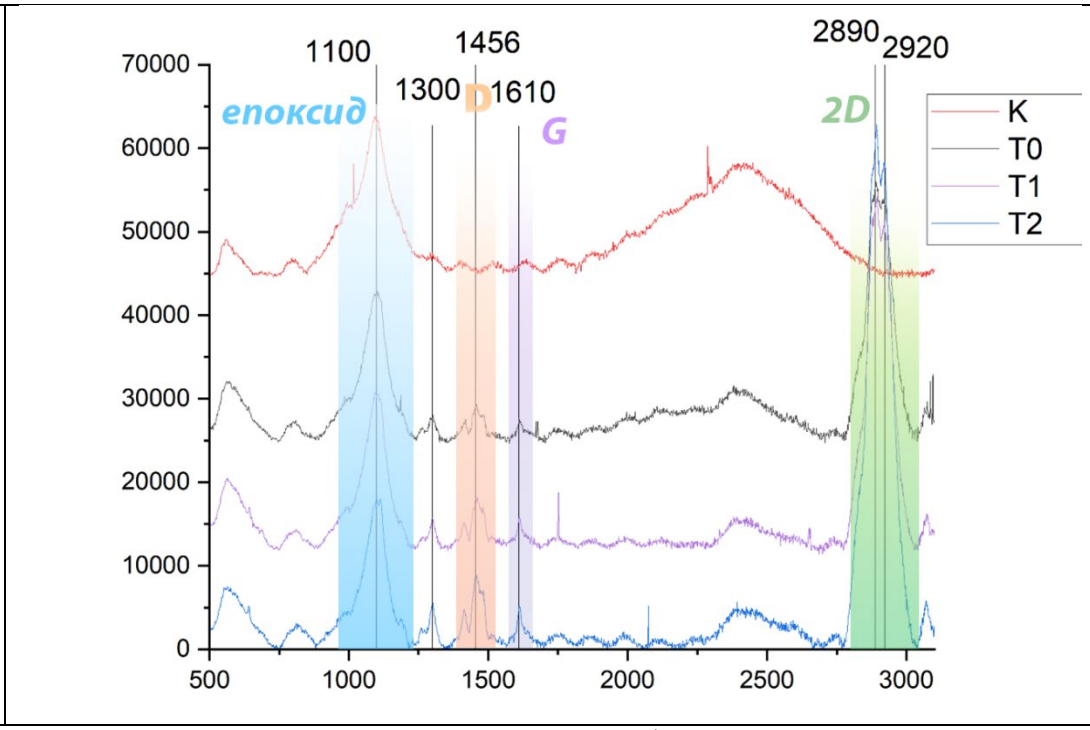

Figure 38. Raman shifts of samples K, T0, T1, T2.

Both the absence of shifts and the identity of the band shapes are categorically confirmed. This eliminates the need for deconvolution and additional mathematical analysis.

Main conclusions from the Raman spectroscopy study:

- The obtained signal corresponds in shape to expectations based on the literature review.
- The lack of shifts between samples indicates a negligible influence of the structure and number of GPL layers.
- The change in intensities is most likely due to a higher concentration of the stable fraction in the suspension, which has significant implications for further studies.
- It is important to note that the liquid samples did not give a good enough signal for processing.
- Although GPL concentrations comparable in order to those used in other studies, it would be beneficial to increase them to make the signal more distinct.

Delamination test results.

The addition of additional components to the coating carries the risk of hindering polymerization and adhesion to the substrate. In addition, one of the objectives of the study is to utilize a polymer that has fallen out of production and to prevent its scrapping by finding alternative applications.

For this purpose, it is necessary to study the mechanical properties of the coating and in particular – adhesion and delamination resistance.

One of the main concerns with the chosen test method is the operator approach. The study in this case was conducted by the author after many years of experience in applying the method in production conditions. It is important to note that in practice the coating is applied to polymer products, while the current study is on glass substrates. Of greatest importance in such a case will be the comparison between the control sample K, which represents the coating on a glass substrate without GPL additives on the one hand, and the sample T0, which represents the coating with added GPL. Samples T0, T1 and T2 should be compared separately, as they show a change in the concentration of dry polymer in the coating.

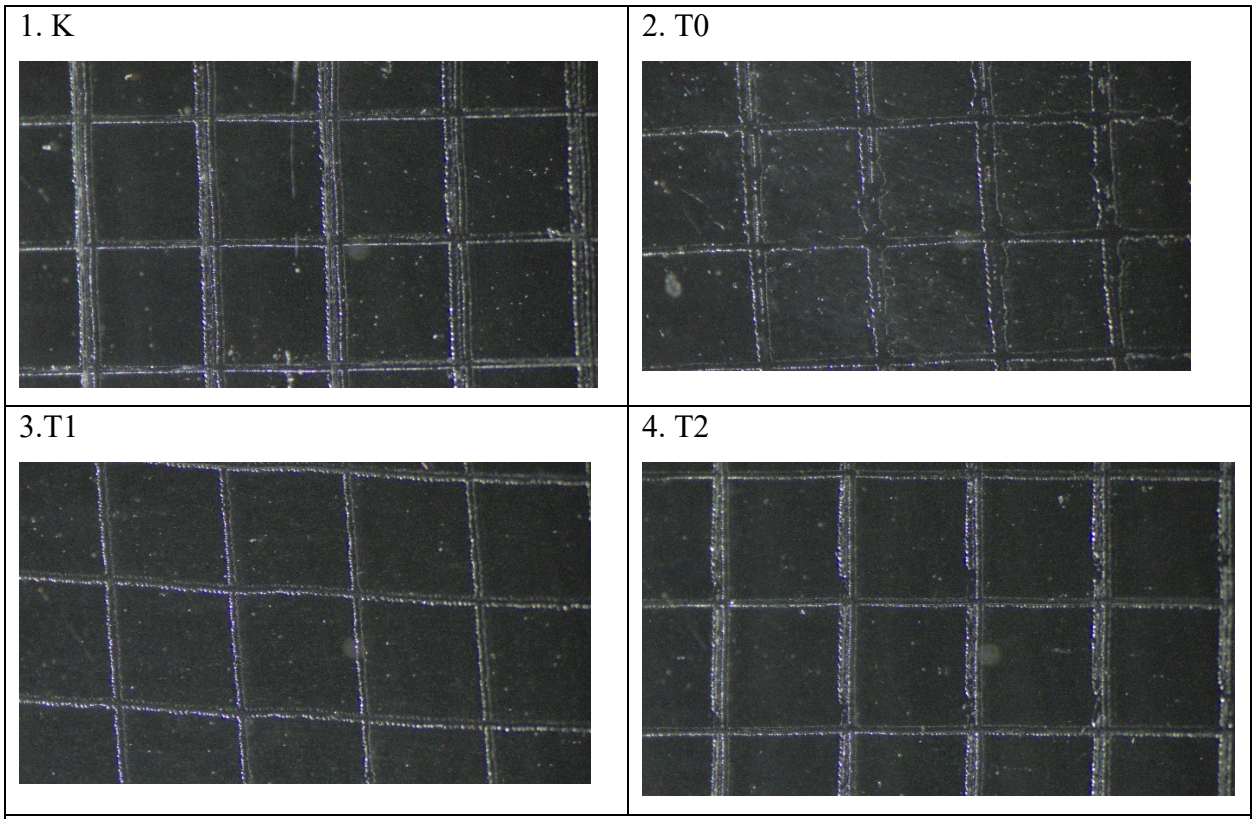

Figure 39. Cross-hatch test according to ASTM: 1. K, 2. T0, 3. T1, 4. T2.

The cross-hatch test highlights the following conclusions:

1. All coatings except sample T0 can be categorized as level 5 or 4.
2. Coating T0 shows delamination parallel to the grooves with a length of more than 1.6mm, therefore it falls into level 2.
3. The results do not show correlative behavior with respect to the varied factors:

- Comparing the control sample K with samples T0, T1 and T2, it cannot be stated that the addition of GPL improves or worsens the mechanical resistance of the coating.
- Comparing the three samples with the participation of GPL among themselves – T0, T1 and T2, it cannot be stated with certainty whether the variation of the dry matter concentration leads to a deterioration in the mechanical resistance of the coating.

Antimicrobial activity test by the agar diffusion method.

The studies were conducted at the Department of Biotechnology at the UCTM. No classical zones of inhibition were observed. The results suggest that the GPL sheets are tightly crosslinked in the polymer matrix and immobilized, therefore they do not diffuse into the agar. On the one hand, this invalidates the antimicrobial properties, but on the other hand, it has the advantage that the active additives in the coating will not enter the environment. In view of these results, two potential approaches are outlined:

- Conducting microbial resistance studies by another method – for example, by immersion in an aqueous environment to study the resistance to fouling by unicellular and multicellular algae, cyanobacteria and other biofilm-forming organisms. Such coatings may find applications as marine coatings.
- Investigation of the stabilizing role of GPL in epoxy coatings to prevent leaching of active components into the environment.

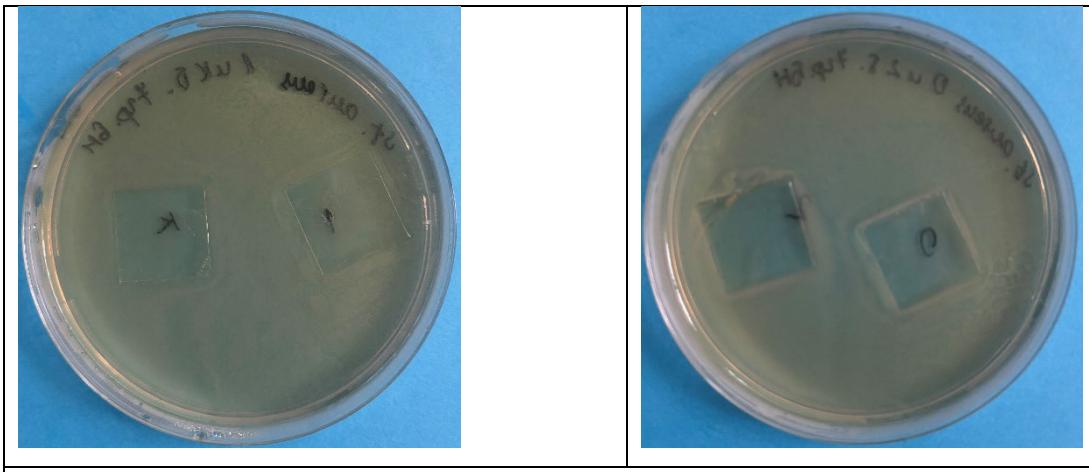

Figure 40. *S. aureus* NBIMCC 3703, samples K, T0, T1, T2

Figure 40 shows the lack of formation of inhibition zones and partial growth on samples K and T1.

7.4.EPOXY COATINGS WITH GO, GPL AND $ZnTiO_3$

In view of the promising preliminary results of antimicrobial activity of zinc titanate, it was selected for the next series of coatings with potential antifouling action. The main objective of the study is to determine the morphology of composites between graphene materials (GO, GPL) and zinc titanate - how the different particles are distributed and whether sufficiently stable dispersions can be obtained for inclusion in polymer coatings. Due to the presence of a larger number of unreduced functional groups on the surface of the graphene layers in GO compared to GPL, we expect the added ZnTiO3 particles to exhibit different behavior when attaching to the surface. To select the material that leads to reduced aggregation of nanosized zinc titanate particles, a series of compositions comparing GO and GPL was developed, which were characterized by TEM.

Table 11. Mass ratios of studied coatings.

Sample	Epoxy	$ZnTiO_3$	GPL	GO
1.	**10**	**0**	**0**	**0**
2.	**9**	**1**	**0**	**0**
3.	**9**	**0**	**1**	**0**
4.	**9**	**0**	**0**	**1**
5.	**9**	**1**	**1**	**0**
6.	**8**	**1**	**0**	**1**

The selected additives – GO, GPL, ZnTiO3 are initially sonicated in methanol to obtain a suspension. To separate the stable fraction, the samples are centrifuged for 15 min at 4000 rpm. The samples are carefully decanted and added to the BPA-ECH solution in the ratios in Table 4. Stir with a magnetic stirrer for 2 min., making sure that no air bubbles form on the surface. The solution is allowed to "rest" for 1 min or until the bubbles disappear. Coatings are applied to glass substrates by dip coating. The removal rate is essential for the thickness and uniformity of the coating. For the purposes of these preliminary studies, the application was done manually, but taking into account the wide application of the method and the epoxy resin used, the use of industrial equipment is very affordable. After application, the samples were placed in a preheated drying oven at 100ºC for 1 hour. The obtained samples were characterized by SEM and TEM. The reaction scheme is shown in Fig. 41. It should also be taken into account the pre-treatment of the substrates using a methodology similar to that described in Fig. 1.

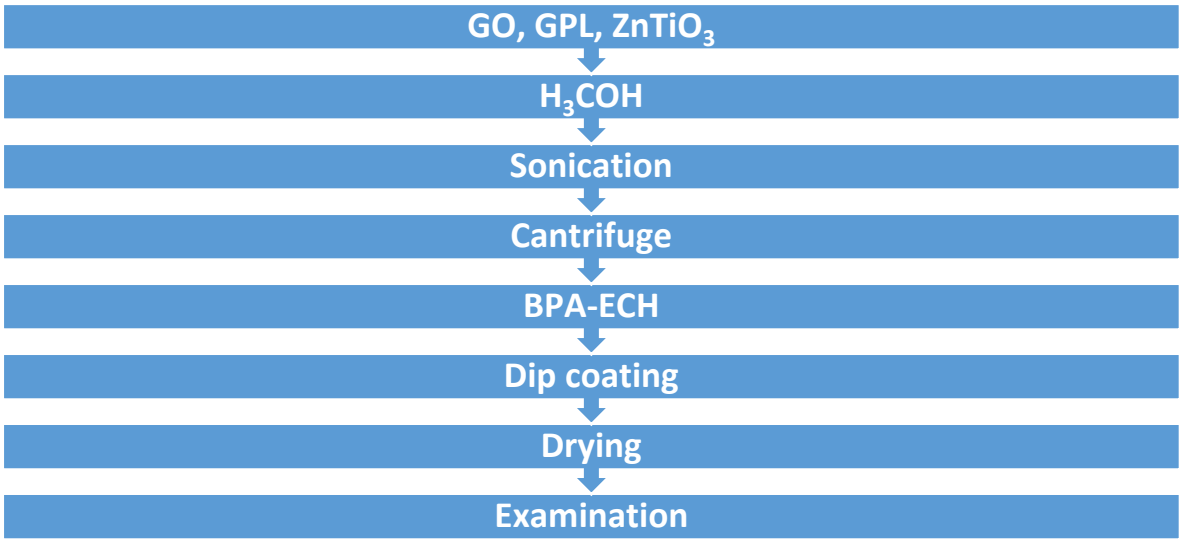

Figure 41. Route for the production of epoxy coatings with GO, GPL, ZnO, and $ZnTiO_3$.

Structural characteristics of the produced coatings

TEM of coatings containing BPA, GO, RGO and $ZnTiO_3$.

From the analysis of the TEM results (Fig. 42 and 43) it was concluded that the ZnTiO3 nanoparticles were evenly distributed in the polymer matrix and the presence of graphene nanostructures was proven. TEM showed that in the compositions with the participation of GO, the sizes of the ZnTiO3 nanoparticles of the order of 10 nm were preserved. It was proven that the ZnTiO3 nanoparticles are stable, evenly distributed in the polymer matrix of the epoxy coating and attach to the surface of the GO and GPL nanolayers.

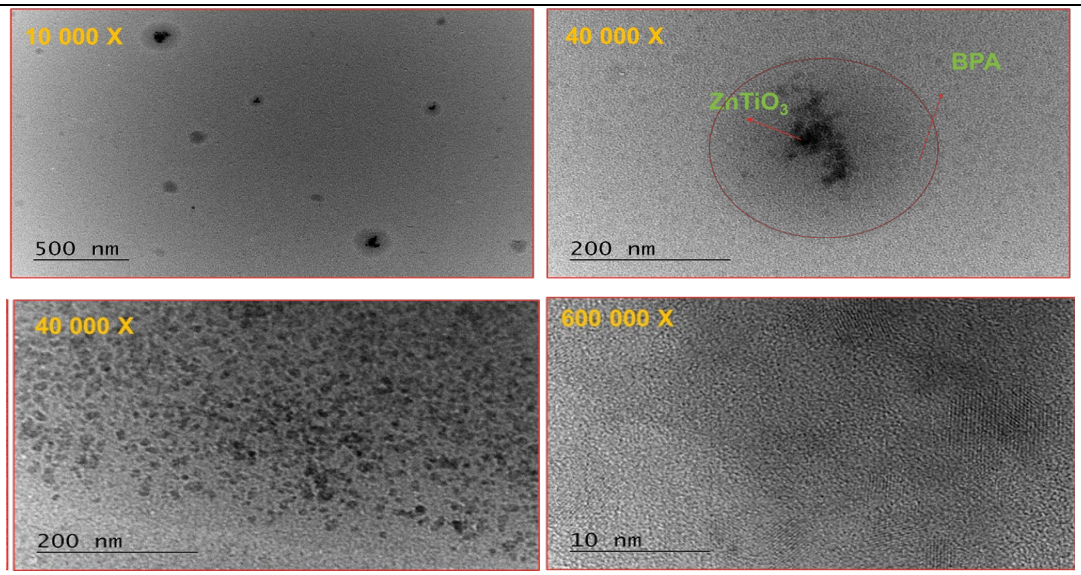

Figure 42. TEM of coating BPA + GO + $ZnTiO_3$

In Fig. 71 the coatings with the participation of GO are presented. Spherical clusters of GO particles with different sizes, varying in the order of 10 and 100nm, are observed. The ZnTiO3 particles are predominantly located on the surface of the graphene layers. It can be concluded that the GO layers influence the dispersion of the oxide nanoparticles and can be used for spatial functionalization of the coatings - with sufficiently good dispersion, homogenization can be achieved. The concentrations of the additives are low, but nevertheless a certain degree of agglomeration of the GO layers is observed. The proposed approach from p. 7.3. for increasing the viscosity of the epoxy resin can also be applied to composite compositions in order to improve their dispersion and thus improve the properties of the coating.

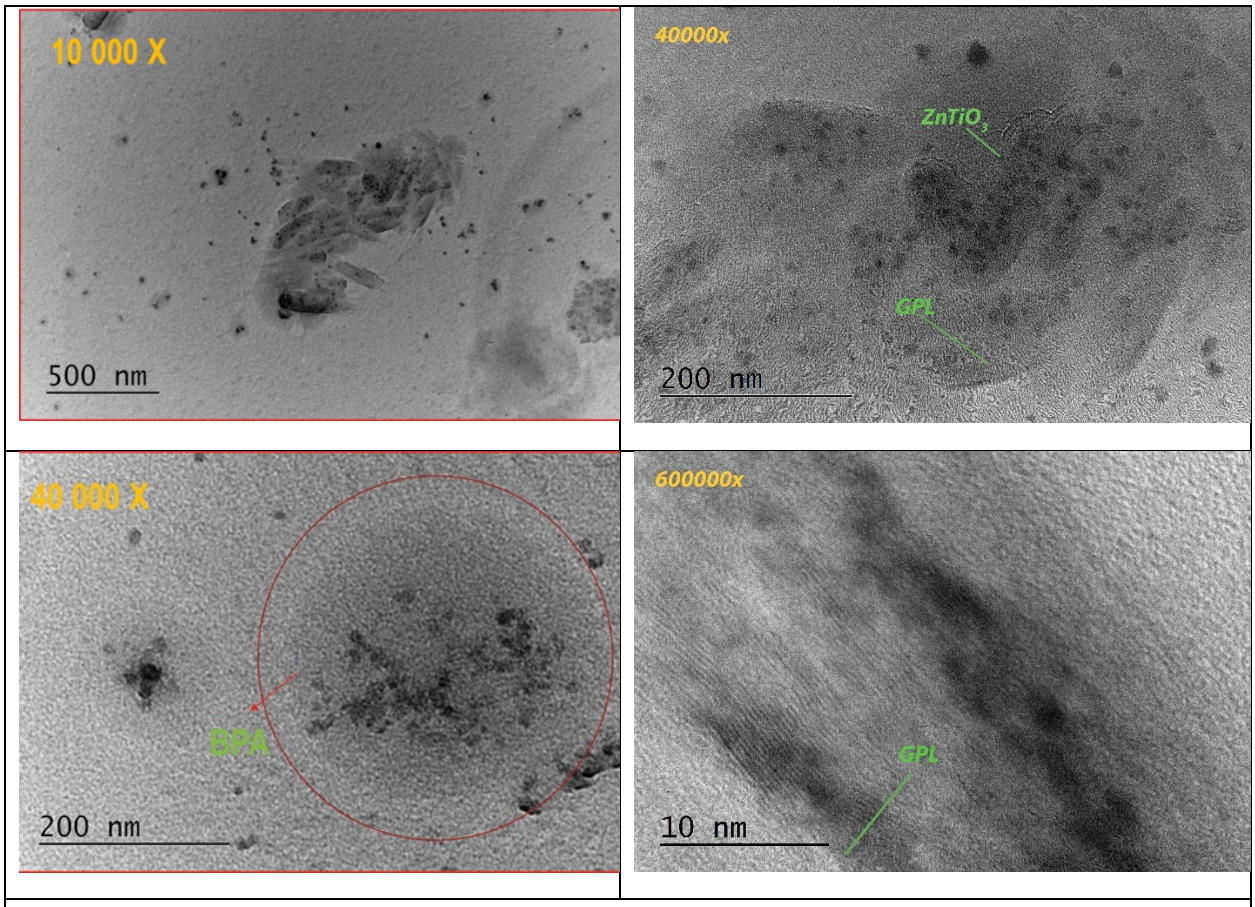

Figure 43. TEM of coating BPA + GPL + $ZnTiO_3$

Fig. 43 presents the compositions with the participation of GPL. Again, the $ZnTiO_3$ particles are directed towards the areas with the presence of graphene materials, as in this case their aggregation is prevented to a greater extent and nanoparticles are observed evenly spaced from each other. Adsorption on the surface of the GPL layers solves the problem of agglomeration of nanosized $ZnTiO_3$ particles, as again the key challenge remains the dispersion of graphene materials in the composition of the composites.

The obtained coatings were again subjected to a study for activity against *S. aureus* and *E. coli* at the Department of Biotechnology of UCTM.

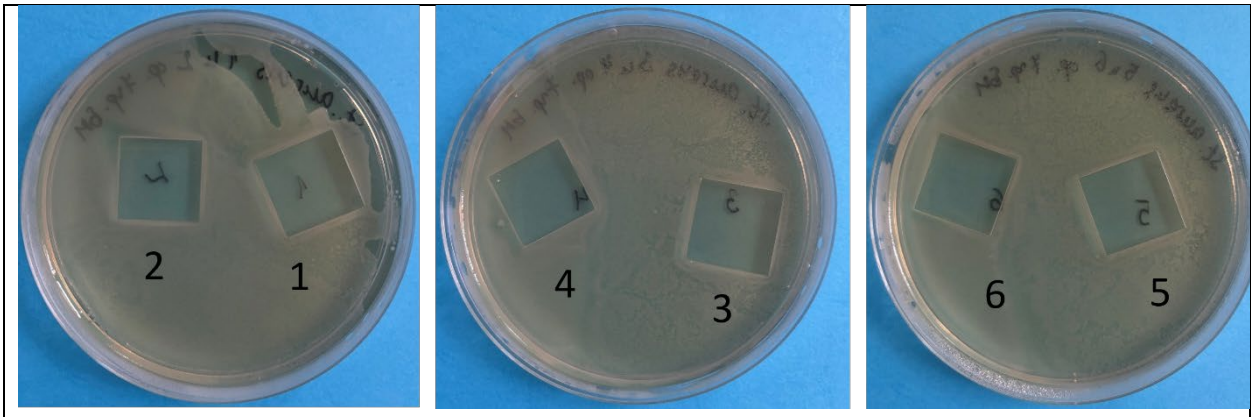

Figure 44. *S. aureus NBIMCC 3703 orange,* samples 1,2,3,4,5,6

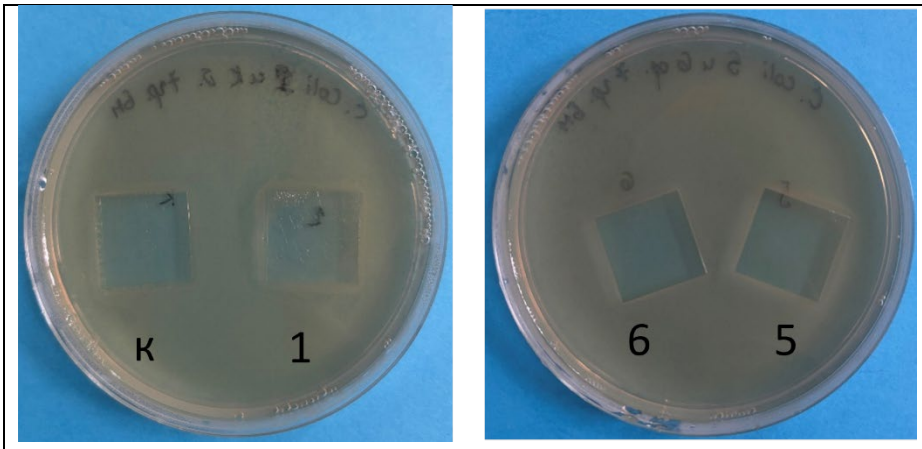

Figure 45. *E. coli* NBIMCC 8785 к,1-white, 5,6-orange

No inhibition zones are observed. This result leads to the interpretation that the nanosized zinc titanate particles and graphene nanoplatelets are tightly bound and intercalated in the polymer matrix and do not exhibit sufficient mobility to diffuse into the medium. Additional studies of similar samples in liquid media are possible to assess their fouling by biofilm-forming microorganisms, unicellular and multicellular algae. Another possible approach is to decorate the nanosized additives on the applied coating before polymerization to provide a free active surface. A third possibility is to increase the concentration of additives to assess the capacity of the epoxy to immobilize the particles.

CONCLUSIONS

1. 1. Original compositions of thin-film optical coatings were obtained using the Electron Beam Physical Vapor Deposition (EBPVD) method.
    1.1. It has been proven that thin layers of SiO_2, Ti_3O_5 and ZrO_2 with thicknesses of the order of tens of nanometers can be obtained by Electron Beam Physical Vapor Deposition (EBPVD), with thicknesses that can be controlled to the order of ±1 nm.
    1.2. It has been proven that by using rows of the thin layers thus obtained, thin-film optical coatings with predefined optical behavior – transmittance and reflectance at certain wavelengths in the visible spectrum $\lambda \in 400 \div 700$ nm can be obtained.
    1.3. The use of quarter-wave thicknesses is an approachable way to calculate the required thicknesses of thin layers that are included in coatings.
    1.4. Original compositions of optical thin-film coatings with the participation of SiO_2, Ti_3O_5 and ZrO_2 have been obtained, the optical properties of which correspond to previously set and theoretical expectations. This has been proven by comparing the experimental curves obtained with a spectrophotometer with the theoretically calculated ones.
    1.5. The possibility of replacing Ti_3O_5 with ZrO_2 in the composition of thin-film optical coatings while maintaining the specified optical properties has been proven.
2. New silicone coating compositions with the participation of graphene materials have been obtained
    2.1. New compositions of silicone composites with the participation of 1, 3 and 5 % additives of GO, RGO, ZnO and ZnO/(5 %) RGO in the form of coatings on glass substrates were obtained.
    2.2. XRD has proven the presence of silicone rubber in all samples, as well as RGO and ZnO in the respective composite compositions. The size of ZnO nanoparticles in the composites containing them has been determined using the QualX computer program (silicone composite with 5% ZnO – 18 nm and silicone composite with 5% [ZnO/(5%)RGO] – 28 nm).
    2.3. The silicon composites with 5% dopant were investigated using SEM and conclusions were drawn regarding the dispersion of graphene structures in the silicon matrix. Agglomerates of ZnO and RGO were observed, distributed over the compact structure of the silicon matrix.
    2.4. The microstructure of the well-separated carbon layers of RGO and elongated ZnO nanocrystals, evenly distributed in the silicon matrix, was observed by TEM analysis.

2.5. From the SAED study of a silicone composite with 5% ZnO and 5% ZnO/(5%) RGO, a conclusion was made about the structure of the ZnO nanocrystallites and the type and parameters of the crystal lattice were determined (Zincite hexagonal, a= 3.24900 Å, c= 5.20700 Å, #96-901-1663).

2.6. The antibacterial activity of the obtained silicone composites against Escherichia coli and Staphylococcus aureus bacteria was investigated using the agar diffusion method. In the case of a silicone composite containing 3% GO (GO3) in the silicone matrix, contact inhibition against Staphylococcus aureus bacteria was observed. And contact killing against the same bacteria was established in the silicone composites with a composition of 1 mass % ZnO (Zn1), 1 and 3 mass % ZnO/5 %RGO (ZR1 and ZR3). Additional studies of the antibacterial properties using other methods are pending

3. Epoxy coatings with the participation of GPL were obtained and the influence of the viscosity of the polymer matrix on the dispersion and delamination of the GPL layers was studied.

3.1. When the concentration of epoxy resin varies, the viscosity changes, which affects the dispersed graphene materials.

3.2. Better preservation of the delaminated layers is obtained at a higher resin concentration, and TEM shows stabilized separated single graphene layers.

4. Epoxy coatings with the participation of GO, GPL and $ZnTiO_3$ were obtained.

4.1. A suitable scheme has been developed for obtaining original compositions of epoxy coatings with the participation of GO, GPL and $ZnTiO_3$.

4.2. The microstructure of well-separated carbon nanosheets of GO and GPL decorated with nanosized $ZnTiO_3$ is observed by TEM.

4.3. It has been shown that $ZnTiO_3$ nanoparticles are stable, uniformly distributed and attach to the surface of graphene sheets.

4.4. GO and GPL were found to successfully prevent agglomeration of nanosized $ZnTiO_3$ particles.

SCIENTIFIC AND APPLIED CONTRIBUTIONS

1. **1. A methodology for obtaining optical coatings with specified optical properties – high transmittance, reflective properties – position, intensity and width of the reflection peak using the Electron Beam Physical Vapor Deposition (EBPVD) method is proposed. A scheme for processing the substrates before applying thin-film optical coatings is improved..**
2. **A procedure for replacing Ti3O5 with ZrO2 in the composition of multilayer optical coatings while maintaining the optical properties within the scope of the assignment is proposed, and methods for compensating for the emerging differences in the optical behavior of the coatings are proposed..**
3. **Original compositions of nanocomposites based on silicone rubber with the participation of RGO and nanosized ZnO in different ratios were obtained. The antimicrobial properties of all compositions were studied and the most active of them were determined - GO3, Zn1, ZR1, ZR3.**
4. **The properties of GO and GPL for association with nanosized ZnTiO3 particles were compared and it was shown that in the presence of GPL the nanoparticles were more stable and resistant to aggregation.**
5. **The influence of the viscosity of the polymer matrix on the delamination of the graphene layers and the stability of the suspension was evaluated.**

PUBLICATIONS CONCERNING THE DISSERTATION

- Staneva AD, **Dimitrov DK**, Gospodinova DN, Vladkova TG**.** Antibiofouling Activity of Graphene Materials and Graphene-Based Antimicrobial Coatings, Microorganisms. 2021;9. https://www.mdpi.com/2076-2607/9/9/1839
- B. L. Martinov, T. E. Vlakhov, A. D. Staneva, S. Slavov, **Dimitar Dimitrov**, Y. G. Marinov, G. B. Hadjichristov, Synthesis and characterization of nanosized ZnTiO3 doped with of reduced graphene oxide (RGO), Journal of Physics: Conference Series 1762 (2021) 012031 doi:10.1088/1742-596/1762/1/012031 - SJR 0.227
- Boris Martinov, Stanislav Slavov, Anna Staneva, **Dimitar Dimitrov**, Janna Mateeva, Electric properties of new composites materials based on RGO, nanosized ZnO and Cu nanoparticles, Journal of Physics: Conference Series, 1762 (2021) 012029 doi:10.1088/1742-6596/1762/1/012029 - SJR 0.227
- D. Dimitrov**, A. Staneva, Effects of epoxy matrix viscocity on the dispersion of GPL graphene layer separation for coatings applications, Journal of Chemical Tehcnology and Metallurgy, in Press**

  Citations – **33:**

  Cited article: Anna D. Staneva, Dimitar K. Dimitrov, Dilyana N. Gospodinova, Todorka G. Vladkova, Antibiofouling Activity of Graphene Materials and Graphene-Based Antimicrobial Coatings, Microorganisms, Sep. 2021, 9(9), 1839; 1-20. https://doi.org/10.3390/microorganisms9091839 ISSN: 2076-2607
  https://www.scopus.com/results/results.uri?s=ref%282-s2.0-85113989556%29&sot=cite&sdt=a&origin=AuthorProfile&src=s&sort=plf-f&limit=10&sessionSearchId=a32363b2173328813830e901db72129b

CONFERENCES

(Titles are in the language in which they were presented)

1. **Dimitar Dimitrov**, Anna Staneva, Tina Tasheva, SYNTHESIS AND APPLICATION OF THIN FILMS IN OPTICS, XVIII Научна постерна сесия за млади учени, докторанти и студенти, Химикотехнологичен и металургичен университет, София, 25 юни, 2021, Сборник с резюмета, стр. 91
2. **Димитър Димитров**, Мария Пенева, Борис Мартинов, Анна Станева, СИЛИКОНОВИ КОМПОЗИТИ С УЧАСТИЕ НА RGO И НАНОРАЗМЕРЕН ЦИНКОВ ОКСИД, XIX Научна постерна сесия за млади учени, докторанти и студенти, Химикотехнологичен и металургичен университет, София, 17 юни, 2022, Сборник с резюмета, стр. 74. https://mmu2.uctm.edu/poster_sessions/XIX/sites/default/files/XIX_Poster_Session_BookOfAbstracts_1.pdf
3. **Д. Димитров**, Заместване на ZnO_2 с Ti_3O_5 в тънкослойни оптични покрития; IX Научна ePoster сесия за студенти и млади учени по случай Деня на металурга;
4. Anna Staneva, Boris Martinov, Janna Mateeva, **Dimitar Dimitrov**, One step synthesis and characterization of RGO/Au NPs nanocomposites, Poster Presentation, NanoSpain2023, April 25-28, 2023 Tarragona (Spain), https://phantomsfoundation.com/NANOSPAINCONF/2023/Abstracts/2023_Staneva_Anna_7.pdf
5. Boris Martinov, **Dimithar Dimitrov**, Anna Staneva, SILICONE COMPOSITES WITH RGO AND NANOSIZED ZINC OXIDE, Poster Presentation, nanoSpain 2023, April 25-28, 2023 Tarragona (Spain), https://phantomsfoundation.com/NANOSPAINCONF/2023/Abstracts/2023_Martinov_Boris_8.pdf
6. Таня Робертова, Борис Мартинов, Жанна Матеева, **Димитър Димитров**, Анна Станева, Едноетапен синтез и охарактеризиране на RGO/Au NPs нанокомпозити, One step synthesis and characterization of RGO/Au NPs nanocomposites, XX Научна постерна сесия за млади учени, докторанти и студенти, Химикотехнологичен и металургичен университет, София, 23 юни, 2023, стр. 74 https://mmu2.uctm.edu/poster_sessions/XX/sites/default/files/XX_Poster_Session_Book OfAbstracts.pdf
7. **Dimithar Dimitrov**, Boris Martinov, Iliana Ivanova, Anna Staneva, ANTIBACTERIAL PROPERTIES OF SILICONE COMPOSITES WITH RGO AND NANOSIZED ZnO, Eighth Balkan conference on Glass Science and Technology; 20th Conference on Glass and Ceramics, 25.09 – 27.09 2023, Nessebar, BULGARIA, p. 67
8. **Димитър Димитров**, Борис Мартинов, Виктор Петров, Анна Станева, ДИСПЕРГИРАНЕ НА ГРАФЕНОВ ОКСИД, РЕДУЦИРАН ГРАФЕНОВ ОКСИД И ЦИНКОВ ТИТАНАТ В BISPHENOL-A ЗА ПОЛУЧАВАНЕТО НА ПОКРИТИЯ С ПОДОБРЕНА УСТОЙЧИВОСТ НА МИКРОБНО ОБРАСТВАНЕ, XXI НАУЧНА ПОСТЕРНА СЕСИЯ ЗА МЛАДИ УЧЕНИ, ДОКТОРАНТИ И СТУДЕНТИ, ХИМИКОТЕХНОЛОГИЧЕН И МЕТАЛУРГИЧЕН УНИВЕРСИТЕТ, СОФИЯ, 21

ЮНИ, 2024 г., СБОРНИК С РЕЗЮМЕТА, ISSN 3033-0769, СТР. 58, HTTPS://MMU2.UCTM.EDU/POSTER_SESSIONS/XXI/SITES/DEFAULT/FILES/XXI_POSTER_SESSION_BOOKOFABSTRACTS.PDF

9. **Димитър Димитров**, Радостина Щеринска, Виктор Петров, Борис Мартинов, Анна Станева, XI-та ePoster научна сесия за студенти, докторанти и млади учени, Химикотехнологичен и металургичен университет, София, 08.11.2024, ПОЛУЧАВАНЕ НА ПОКРИТИЯ ЧРЕЗ ДИСПЕРГИРАНЕ НА ГРАФЕНОВ ОКСИД, РЕДУЦИРАН ГРАФЕНОВ ОКСИД И ЦИНКОВ ТИТАНАТ В BISPHENOL-A

10. **Dimitar Dimitrov**, Boris Martinov, Anna Staneva, PREPARATION OF COATINGS BY DISPERSING GRAPHENE OXIDE, REDUCED GRAPHENE OXIDE AND ZINC TITANATE IN BISPHENOL-A, International Conference on Bioactive, Organic and Inorganic Advanced Materials and Clean Technologies (Sofia, Bulgaria 24-28 March 2025)

11.B. Martinov, A. Staneva, **D. Dimitrov**, A. Kostadinova, I. Ivanova, TS. Foteva, V. Nemska, STRUCTURAL CHARACTERIZATION, CITOTOXITY AND ANTITUMOR ACTIVITY OF ONE STEP SYNTHESIZED RGO/Au NPS NANOCOMPOSITES, International Conference on Bioactive, Organic and Inorganic Advanced Materials and Clean Technologies (Sofia, Bulgaria 24-28 March 2025)

12. Boris Martinov, **Dimithar Dimitrov**, Tanya Robertova, Anna Staneva, STABILIZATION OF Au NPS AND RGO/Au NPS NANOCOMPOSITES FOR APPLICATION IN BIOMEDICINE, International Conference on Bioactive, Organic and Inorganic Advanced Materials and Clean Technologies (Sofia, Bulgaria 24-28 March 2025)

THESIS CONSULTANCY

(Titles are in the language in which they were presented)

1. Мария Пенева:„Силиконови композити с участие на графенови материали и наноразмерен цинков оксид“, магистър, ХТМУ, Катедра „Технология на силикатите“, № ММ 0628, Март, 2022 г.
2. Мария-Габриела Желева – “Проблеми възникващи при електроннолъчево физическо парофазово отлагане на тънкослойни оптични покрития”, бакалавър, Пловдивски Университет „Паисий Хилендарски“, Катедра „Инженерна физика“
3. Виктор Петров – „Полимерни покрития с участието на графенов оксид, редуциран графенов оксид, метални и оксидни наночастици”, магистър, ХТМУ, Катедра „Технология на силикатите“, фак.№ ММ0755, Март, 2025 г.